Accepted Manuscript

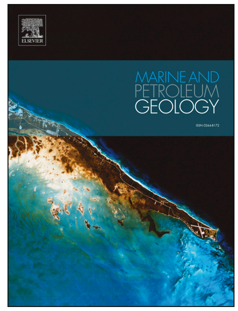

Burial and exhumation history controls on shale compaction and thermal maturity along the Norwegian North Sea basin margin areas

Irfan Baig, Jan Inge Faleide, Nazmul Haque Mondol, Jens Jahren

PII: S0264-8172(19)30100-X

DOI: https://doi.org/10.1016/j.marpetgeo.2019.03.010

Reference: JMPG 3751

To appear in: *Marine and Petroleum Geology*

Received Date: 23 May 2018

Revised Date: 6 March 2019

Accepted Date: 10 March 2019

Please cite this article as: Baig, I., Faleide, J.I., Mondol, N.H., Jahren, J., Burial and exhumation history controls on shale compaction and thermal maturity along the Norwegian North Sea basin margin areas, *Marine and Petroleum Geology* (2019), doi: https://doi.org/10.1016/j.marpetgeo.2019.03.010.

Burial and exhumation history controls on shale compaction and thermal maturity along the Norwegian North Sea basin margin areas

Irfan Baig[1,], Jan Inge Faleide[1], MD Nazmul Haque Mondol[1,2], Jens Jahren[1]*

[1] Department of Geosciences, University of Oslo, Norway

[2] Norwegian Geotechnical Institute (NGI), Oslo, Norway

Abstract

The North Sea area has been subjected to significant erosion and subsequent deposition of sediments in the basin margin and deeper basin areas, respectively, during the late Neogene. A large amount of Cretaceous-early Quaternary sediments have been removed below the angular unconformity along the west and southwest coast of Norway and deposited in the huge North Sea Fan at the mouth of the Norwegian Channel. At the same time, a considerable thickness of early Quaternary-Paleocene sediments was also eroded towards the east in the central North Sea and subsequently deposited in the deeper basin areas to the west. This study seeks to estimate exhumation from compaction and thermal maturity based techniques by using sonic velocities of shales/carbonates and vitrinite reflectance data in a large number of boreholes in the central, eastern and northern North Sea. The results indicate no or minor exhumation in the Central Graben and flanking high areas, whereas more than ~1 km sediments are eroded in the basin margin areas towards the Norwegian coast. More than ~500 m sediments are eroded in the Egersund Basin and Stord Basin areas. A similarity of exhumation estimates from the Early Cretaceous-Early Miocene shales and Late Cretaceous-Early Paleocene carbonates indicates maximum burial sometime after the Early Miocene in most of the central and northern North Sea areas. However, the maximum burial throughout the North Sea Basin may be diachronous. Seismostratigraphic analysis indicates maximum burial sometime during the Oligocene in the Sorgenfrei-Tornquist Zone area in the eastern

North Sea. Maximum burial in the Norwegian-Danish Basin varies from Miocene-Pliocene in eastern parts to early Pleistocene in western parts, whereas sediments are currently at their maximum burial in the Central Graben and southern Viking Graben areas. Restoration of surface elevations to their original position before the onset of erosion indicated large subaerially exposed areas in the Norwegian-Danish Basin and along the southwest coast of Norway. This is also supported by predominantly coastal and/or deltaic environments in the Norwegian-Danish Basin area during the late Neogene. These subaerially exposed areas may be linked to the regional tilting and erosion of the basin margin areas to the east and progressive basinward migration of deposition centres to the west since the Oligocene. The exhumation had significant effects on the petroleum system in the basin margin areas by cooling down the source rock. However, the deeper burial of sediments may also have changed the rheological properties of sediments from more ductile to brittle due to compaction and diagenetic processes which makes them more failure prone during exhumation leading to hydrocarbon leakage or seal failure in case of CO_2 injection.

Keywords: burial; exhumation; compaction; subsidence; thermal maturity; basin analysis; North Sea

1. Introduction

The North Sea is a large sedimentary basin formed as a result of multiple rift phases predominantly during the Late Permian-Early Triassic and Late Jurassic-Early Cretaceous (Ziegler, 1975, 1978; Faleide et al., 2010). The North Sea Basin is the most prolific hydrocarbon province of the North Atlantic rift, but hydrocarbon exploration on the North Sea margin is still very sparse due to a limited number of wells drilled with unsuccessful results and poor understandings of the petroleum system (Armour et al., 2003). Identification of elements of a working petroleum system is crucial for successful hydrocarbon exploration in any area (Underdown et al., 2007). A critical aspect of petroleum system modelling is an estimation of eroded overburden for studying the timing of source rock maturation, expulsion and trapping of hydrocarbons (Doré and Jensen, 1996; Underdown et al., 2007; Marcussen, 2009). The burial and exhumation histories are also crucial for understanding compaction and diagenetic processes due to its significant effects on the source, reservoir and seal rock properties (Henriksen et al., 2011; Baig et al., 2016). The passive continental margins of the North Atlantic region have been subjected to different episodes of extensive post-Triassic exhumation. The timing, causes, and magnitudes of these exhumation episodes are still uncertain and debated in the literature, (e.g. Doré et al., 2002; Anell et al., 2009; Edward, 2011). Many previous workers have highlighted the importance of exhumation in the North Sea associated with the mid-Jurassic regional doming of the North Sea and mid-Cenozoic tectonic activities along the North Sea margins (Ziegler, 1990a; Japsen, 1993; Faleide et al., 2002; Japsen et al., 2007). The late Cenozoic uplift in the eastern Norwegian North Sea is estimated to be ~1-2 km from compaction and thermal maturity data (Jensen and Schmidt, 1993; Japsen, 1999; Japsen and Bidstrup, 1999; Japsen et al., 2008; Japsen et al., 2010).

Many authors have described the source to sink relationship for the pre-Quaternary strata sourced from southern Norway and deposited in the basin areas (Eidvin et al., 1993; Eidvin et al., 1998; Rundberg and Eidvin, 2005; Eidvin and Riis, 2013; Jarsve et al., 2014a). However, the link between sediments eroded in the nearshore areas and redeposited in the offshore areas is also an essential factor that should be considered for the later evolution of the North Sea Basin. Quaternary and pre-Quaternary strata are strongly tilted below a distinct angular unconformity dated to be ~1.1 Myr old, at the base of the Norwegian Channel along the west and southwest coast of Norway (Sejrup, 1995). Paleocene to early Quaternary strata is also truncated below the mid-late Quaternary glacial sediments in the Norwegian-Danish Basin area and further east in the platform areas (Fig. 1). This unconformity is interpreted to be developed as a result of repeated shelf edge glaciations during the last ~0.45 Myr, and it may have reworked the older unconformities (Sejrup et al., 2005; Nielsen et al., 2008). The timing of maximum burial depth and uplift/erosion is still not certain in the North Sea Basin margin areas. It is also unclear what type of sediments were present before the uplift/erosion in these areas. This requires looking further back in time as well as into the areas currently at their maximum burial depth to delineate the sedimentary environments/processes that were active during the Quaternary and pre-Quaternary periods and to get a detailed burial history for a better understanding of the hydrocarbon maturation, generation, migration and distribution in the basin margin areas.

In this study, burial and thermal histories are presented from the analyses of sonic velocity and vitrinite reflectance data in the Norwegian North Sea Basin. The objective of the study is to quantify the amount of exhumation and to investigate the effects of burial and exhumation on rock properties and source rock maturity. The aim is also to create a link between the onshore and offshore geology as well as between missing sediments in the basin margin areas and subsequent deposition in the basin areas. Paleo-pore pressure and paleotemperature are also modelled to discuss the implications of uplift and erosion for regional geology and hydrocarbon exploration.

The magnitude of uplift and erosion is defined in different ways, e.g. gross exhumation and net exhumation. Therefore, it should be noted that compaction and thermal maturity techniques used in the current study estimate net exhumation which is the difference between maximum burial depth and present-day burial depth of a specific unit, whereas gross exhumation is the sum of net exhumation and thickness of post-exhumation sediments (Corcoran and Doré, 2005). The magnitude of net exhumation estimated from the compaction/thermal maturity techniques would be equal to the gross exhumation if there is no post-exhumation reburial of the sediments. In contrast, if the thickness of post-exhumation reburial is more than the gross exhumation, then compaction/thermal maturity techniques will not estimate any uplift and erosion. Net exhumation estimates are important for predicting rock properties while gross exhumation estimates are essential for modelling burial and thermal histories of a basin.

A different nomenclature for the last ~2.6 Myr is used in the previously published studies. Gelasian stage (~2.6-1.8 Ma) was part of Upper Pliocene, but in the new time scale, it is now included in the Pleistocene. Therefore, the age data for the Upper Pliocene documented in the previously published literature are converted into the currently used geological time scale of Cohen et al. (2013).

2. Geological setting

The North Sea is a large sedimentary basin covering a wide area of northwestern Europe. The North Sea Basin consists of deep Cretaceous sub-basins in the central areas (e.g. Central Graben and Viking Graben) flanked by basin margin highs and platform on either side of these sub-basin centres (Fig. 2). The North Sea Basin formed as a result of multiple rift phases, particularly during the Permian-Early Triassic and Late Jurassic-Early Cretaceous (Ziegler, 1975, 1978). Most of the graben structures in the central and northern North Sea developed during the Late Jurassic-Early Cretaceous rifting (Gabrielsen et al., 1990; Ziegler, 1990b). The post-rift shift from continuous siliciclastic to mainly chalk deposition occurred during thermal subsidence in Late Cretaceous to Early Paleocene in the central North Sea (Fig. 1), whereas deposition of siliciclastics continued in the northern North Sea (Surlyk et al., 2003). The deposition of siliciclastic sediments resumed in early Cenozoic in the central North Sea and continued until Quaternary throughout the North Sea Basin (Fig. 1). The early Cenozoic basin configuration of the North Sea Basin was dominated by enhanced tectonic subsidence during the Late Paleocene-Eocene. The sediments of Paleocene-Eocene Rogaland Group and lower part of Eocene-Early Miocene Hordaland Group were sourced mainly from the uplifted basin margin areas to the west (e.g. uplifted Shetland Platform) and from some local sediment source areas in the western Norway (Jordt et al., 2000; Eidvin and Rundberg, 2001; Faleide et al., 2002; Rasmussen, 2004; Rundberg and Eidvin, 2005). The uplift of southern Norway at the Eocene-Oligocene boundary resulted in a shift from eastward to westward progradation of sedimentary wedges in the central North Sea, whereas major sediment source areas remained to the west in the northern North Sea during this time (Japsen and Chalmers, 2000; Faleide et al., 2002; Anell et al., 2012).

Westward progradation in the central North Sea and eastward progradation in the northern North Sea continued during the Miocene-Pliocene in the upper part of the Eocene-Early Miocene Hordaland Group and lower part of the Middle Miocene-Quaternary Nordland Group (Brekke, 2000; Faleide et al., 2002; Løseth and Henriksen, 2005; Eidvin et al., 2014). The early Quaternary marked a major shift in progradation direction in the northern North Sea when southwestern Norway took over from the East Shetland Platform as a major sediment source area possibly due to deteriorating climatic conditions and/or renewed tectonic activity or combination of both (King, 2016). The early Quaternary sedimentation in the central and northern North Sea was dominated by the progradation of hundreds of meters thick clastic wedges in response to uplift and glacial erosion of eastern source areas (Sejrup et al., 1996; Eidvin and Rundberg, 2001; Faleide et al., 2002; Eidvin et al., 2014; Baig, 2018). A significant uplift and erosion along the northern North Sea basin margin is also indicated by the strong tilting of the entire Cenozoic succession below the mid-late Quaternary glacial unconformity (Riis, 1996; Faleide et al., 2002). Late Neogene uplift in the order of 500-1500 m is also well documented in the Skagerrak area (Jensen and Schmidt, 1992; Japsen et al., 2007).

Ice sheets appeared to have been building up from about 2.7 Ma in the areas adjacent to the North Sea (Eidvin et al., 2000; Kleiven et al., 2002; Mangerud et al., 2011). The ice initially flowed southwards along valleys when the major ice sheets developed in Scandinavia and then, since about 1.1 Ma, continued up along the west coast of southern Norway and eroded a trough, the Norwegian Channel, down to ~700 m depth into the Cenozoic and Mesozoic sedimentary successions (Sejrup, 1995; Sejrup et al., 2003; Baig, 2018). The glacially eroded sediments were transported by the fast flowing Norwegian Channel Ice Stream to the northern North Sea margin and deposited in the North Sea Fan at the mouth of the Norwegian Channel (Sejrup et al., 1996; Nygård et al., 2005; Nygård et al., 2007). The Scandinavian and British ice sheets covered the North Sea area outside the Norwegian Channel on several occasions during the last ~0.45 Myr, and deposited interbedded glaciogenic and fine-grained sediments (Jansen and Sjøholm, 1991; Sejrup, 1995; Eidvin et al., 2000; Sejrup et al., 2000; Stoker et al., 2005).

3. Material and methods

3.1. Data collection and preparation

Wireline log data from more than 260 exploration boreholes from Norwegian Petroleum Directorate and thermal maturity data compiled from geochemical analysis reports from more than 60 exploration boreholes in the Norwegian sector were utilized in this study (Fig. 2). In addition to this, check shot data from nearly 30 boreholes in the Danish sector compiled from Nielsen and Japsen (1991) and data along three depth-converted seismic sections in the Stavanger Platform (Fig. 4 in Riis, 1996) and Stord Basin (Fig. 5 in Riis, 1996 and transect-2 in Fig. 2) areas were also utilized to increase data coverage towards the edges of the study area (Fig. 2). Formation tops, biostratigraphic ages, bottom-hole temperature information, drilling mud, leak off test and drill stem test data were gathered from borehole completion and geochemistry reports. The study area covers different geological provinces in the Norwegian and Danish sectors. Different naming conventions are used for the Early Cretaceous-Triassic stratigraphic units in different regions and therefore, for this reason, all age equivalent lithostratigraphic units were combined into a single group when analysed in this study, e.g. formations within the Viking Group in the Viking Graben area and their age equivalent formations in the Tyne Group in the Central Graben area and Boknfjord Group in the Norwegian-Danish Basin area were grouped under the Viking Group (Fig. 1).

The shales belonging to Early Cretaceous Cromer Knoll Group, Late Cretaceous-Early Paleocene Shetland Group, Paleocene-Eocene Rogaland Group, and Eocene-Early Miocene Hordaland Group were analysed to study the compaction and exhumation processes. The Late Cretaceous-Early Paleocene Shetland Group carbonates in the central North Sea were also analysed as an additional constraint, and exhumation estimates were also incorporated in the final results.

All types of borehole data were imported into the Petrel software. Erroneous log data due to poor borehole conditions or casing were removed. Most of the studied boreholes have gamma ray, sonic, resistivity and caliper logs throughout the borehole sections, whereas bulk density and neutron porosity logs were available mostly in the deeper parts. Shear wave sonic logs were available in only a few boreholes (nearly 30 boreholes). As a starting point, gamma ray, bulk density, and neutron porosity logs were used to group interval transit time/compressional velocity data into different electro-facies (e.g. sands, shales, and carbonates). Log data filtered for only shale and carbonate facies were used for further analysis.

3.2. Compaction analysis

Sonic velocity from sonic logs is most widely used to estimate exhumation in sedimentary basins around the world (Hillis, 1995; Corcoran and Doré, 2005; Mavromatidis and Hillis, 2005; Mavromatidis, 2006; Japsen et al., 2007; Japsen et al., 2008; Dörr et al., 2012; Tassone et al., 2014). Sonic velocity in uniform lithologies such as mudstones/shales is a function of porosity, and it increases with burial depth in hydrostatically pressured and normally compacted sediments (Magara, 1976; Bulat and Stoker, 1987; Hillis, 1995; Menpes and Hillis, 1995; Corcoran and Doré, 2005). Compaction due to burial is considered to be largely irreversible, and sedimentary rocks will, therefore, show anomalously high interval velocity after exhumation due to over-compaction/over-consolidation (Bulat and Stoker, 1987; Hillis, 1995; Menpes and Hillis, 1995; Corcoran and Doré, 2005).

Experimental studies have shown that the evolution of physical properties of sediments during progressive burial depends on the mineralogy and texture of the sediments (Mondol et al., 2007; Fawad et al., 2010). Variation in clay mineralogy and silt content in mudstones may play the most significant role in controlling the physical properties resulting in different normal compaction depth-trends for different lithologies. Higher silt content in mudstones results in poor sorting that leads to higher sonic velocity probably due to more grain-grain contact (Marion et al., 1992). Therefore, different normal compaction depth-trends are required to be established for different lithostratigraphic units analysed in this study (Fig. 3).

In order to calculate maximum burial depth from compaction data, it is usually assumed that sediments are hydrostatically pressured and follow normal compaction trends with increasing burial depth (Hillis, 1995; Menpes and Hillis, 1995). However, a common problem to satisfactorily establish normal compaction trends is the occurrence of overpressure which can cause under-compaction of sediments and hence low velocity-depth gradients (Japsen, 1998). Data from any such overpressured intervals were therefore excluded from the compaction analysis. Previous studies show that the Late Cretaceous-Early Paleocene carbonates are highly overpressured (up to 20 MPa) in the Central Graben area (Caillet et al., 1997; Japsen, 1998). Therefore, the areas with a known overpressure of >5 MPa were also avoided when establishing the normal compaction trends in this study (e.g. overpressured areas shown in the index map in Fig. 4).

Many authors have described an exponential relationship between interval transit time and depth, (e.g. Magara, 1976; Heasler and Kharitonova, 1996; Tassone et al., 2014) similar to porosity depth equations (Athy, 1930; Sclater and Christie, 1980).

$$DT = (DT_o - C) * e^{-bZ} + C \qquad \textit{Eq. 1}$$

where DT is interval transit time through normally compacted uniform lithology, DT_o is the interval transit time at the surface, C is a shift constant or matrix transit time, `b` is a compaction coefficient and Z is the depth below the seafloor. The linear form of the above equation was attained by taking the logarithm of both sides.

$$\ln(DT - C) = \ln(DT_o - C) - bZ \qquad \textit{Eq. 2}$$

Normal compaction curves through shales were categorized into two sets based on observed velocity-depth relationships which indicate different gradients for shallow and deeper burial depths. The reason for establishing separate normal compaction curves as a function of depth was that compaction is governed by stress-dependent mechanical processes (e.g. grain re-arrangement) at shallow depth while at deeper depth temperature and time-dependent chemical compaction (e.g. pressure solution and quartz cementation) dominate (Bjørlykke and

Høeg, 1997). Velocity increases slowly with decreasing porosity and shows narrow spread within the mechanical compaction domain (Fig. 3c). The velocity increases significantly due to cementation as the temperature reaches to > 70–80 °C. A small amount of cement can stiffen the rock framework and increase the velocity significantly (Bjørlykke and Høeg, 1997; Bjørlykke, 1999; Storvoll et al., 2005). Another reason was that lithostratigraphic units currently in the mechanical compaction domain in the reference areas are either very thin or removed in the basin margin areas to the east. Therefore, to utilize sonic velocity data throughout the borehole sections, we need to establish separate normal compaction curves for shallow and deeply buried sediments. Many authors have also used different velocity-depth trends for shallow and deeply buried intervals (Japsen, 1998; Japsen et al., 2002). As a starting point to separate the shallow and deeply buried sediments, the likely transition zone between mechanical and chemical compaction was identified from rock physics templates and bottom hole temperature analyses in the reference areas (Fig. 2). Cross-plot of bulk density/porosity versus shear wave velocity or shear modulus (rock stiffness) is a good approximation for differentiating mechanical and chemical compaction zones (Storvoll and Brevik, 2008). Two separate trends can be identified in the shear modulus and porosity (derived from density log) cross-plots (Fig. 3a). A more flat line and a steeper line represent the mechanical and chemical compactions of the sediments, respectively. Shear modulus changes little in the mechanical compaction zone while porosity decreases rapidly, whereas the porosity loss rate is reduced while shear modulus increases rapidly in the chemical compaction zone. The flatter shear modulus and porosity trends are referred to as depositional trends controlled by sedimentation (e.g. variation in sorting and clay content), whereas the steep trends are representative of porosity controlled by diagenesis, (e.g. pressure solution and cementation) (Avseth et al., 2005). A further breakdown of P-wave velocity between 2200 m/s and 2600 m/s in the shear modulus and porosity cross-plots emphasizes the velocity changes from the mechanical to chemical compaction domains and helps to identify the P-wave velocity cut off value between the two domains. Cross-plot of shear modulus and porosity indicates that the P-wave velocity is less than 2400 m/s (126 µs/ft) and more than 2600 m/s (122 µs/ft) in the zones dominated by mechanical and chemical compaction, respectively (Fig. 3a).

The interval transit time (reciprocal of velocity) data for the Early Cretaceous-Early Miocene shales and Late Cretaceous-Early Paleocene carbonates were extracted, logarithmically transformed and plotted against depth below the seafloor. The least square fitting technique was applied to equation 2 to find different values of compaction coefficients ´b´ for different lithologies in the central and northern North Sea (e.g. Fig. 3b).

The sonic log data were available from a large number of reference boreholes in the Central Graben and south Viking Graben areas (Fig. 2). This enables better control on velocity-depth relationships in this area compared to the uplifted Barents Sea area where only a few wells are drilled in the areas currently at their maximum burial depth (Henriksen et al., 2011; Baig et al., 2016). Sonic log data were grouped into shallow/mechanical compaction domain representing sonic velocity less than 2400 m/s and deeper/chemical compaction domain representing sonic velocity higher than 2400 m/s. A set of separate reference compaction curves were established for the Early Cretaceous-Early Miocene shales and Late Cretaceous-Early Paleocene carbonates in the central and northern North Sea. The sonic data were physically constrained between the near-surface transit time (DT_o) and matrix transit time (shift constant C) to establish reference compaction curves through shales in the shallow regions (Vp <2400 m/s). The compaction coefficient ´b´ was then estimated by drawing the best-fit regression lines through the data (Fig. 3b). Compaction coefficient ´b´ was estimated to be 0.00023 m^{-1} by using the surface and matrix transit times of 177 µs/ft and 66 µs/ft, respectively, for the Eocene-Early Miocene Hordaland shales in the central North Sea (Eq. 3).

For Hordaland shales in the northern North Sea, the compaction coefficient was also estimated to be 0.00023 m^{-1} but by using the surface and matrix transit times of 168 µs/ft and 66 µs/ft, respectively (Eq. 4).

$$DT = 111 * e^{-0.00023Z} + 66 \qquad Eq.\ 3$$

$$DT = 102 * e^{-0.00023Z} + 66 \qquad Eq.\ 4$$

Compaction coefficients through deeper regions (Vp > 2400 m/s) were obtained by statistically optimizing the model described for the shallow regions. In this case matrix values were kept constant at 60 µs/ft for the Cromer Knoll and Rogaland group shales in the central and northern North Sea and 56 µs/ft for the Shetland Group shales in the northern North Sea. However, the surface interval transit time values were changed beyond the physically constrained values to get the higher R^2 values. This approach resulted in two different velocity-depth trends to be used for the shallow and deeper regions. Compaction coefficients `b` for the Paleocene- Eocene Rogaland Group shales were estimated to be 0.00046 m^{-1} by using the surface and matrix transit times of 270 µs/ft and 60 µs/ft, respectively, in the central North Sea (Eq. 5) and 0.00042 m^{-1} by using the surface and matrix transit times of 206 µs/ft and 60 µs/ft, respectively, in the northern North Sea (Eq. 6). Compaction coefficient `b` for the Late Cretaceous-Early Paleocene Shetland Group shales in the northern North Sea was estimated to be 0.00059 m^{-1} by using the surface and matrix transit times of 230 µs/ft and 56 µs/ft, respectively, in the northern North Sea (Eq. 7). The compaction coefficient `b` for the Early Cretaceous Cromer Knoll Group shales was estimated to be 0.00042 m^{-1} by using the surface and matrix transit times of 206 µs/ft and 60 µs/ft, respectively, in both the central and northern North Sea same as in equation 6.

$$DT = 210 * e^{-0.00046Z} + 60 \qquad Eq.\ 5$$

$$DT = 146 * e^{-0.00042Z} + 60 \qquad Eq.\ 6$$

$$DT = 194 * e^{-0.00059Z} + 56 \qquad Eq.\ 7$$

A similar approach was also used to estimate the compaction coefficient through Shetland Group carbonates in the central North Sea. The Shetland Group sediments are penetrated at deeper than 1000 m depth in boreholes currently at their maximum burial depth. Therefore, the normal compaction curve for shallow depths (<1000 m) was adopted from Japsen (2000), and the compaction coefficient for data points at more than 1000 mbsf burial depth was estimated to be 0.00137 m^{-1} by using the surface and matrix transit times of 260 µs/ft and 50 µs/ft, respectively (Eq. 8).

$$DT = 210 * e^{-0.00137Z} + 50 \qquad Eq.\ 8$$

The sonic log data were then calibrated with the established reference compaction curves, and an upward deviation from the reference compaction curves was estimated graphically or mathematically as net exhumation (Eq. 9).

$$Ea = -\frac{1}{b} * ln\left[\frac{DT - C}{DT_o - C}\right] - Z_p \qquad Eq.\ 9$$

Where Ea is the estimated net exhumation and Z_p is the present-day burial depth of the sampled interval transit time DT under consideration in the borehole.

3.3. Thermal maturity analysis

Subsidence of progressively buried sedimentary layers causes the thermal maturation of the sediments. Temperature and time are the most critical factors in the thermal maturation of organic matter. This temperature and time dependency is described by chemical reaction kinetics, which states that the reaction rate increases exponentially with temperature. However, once the material undergoing the thermal maturation is consumed, the reaction rate slows down with the increasing temperature (Waples, 1984; Barker, 1989; Burnham and Sweeney, 1989; Waples, 1994a; Waples, 1994b). The cumulative effect of increasing temperature over time is the measure of burial history and can be evaluated by integrating the reaction rate over time (Allen and Allen, 2013). Many different indicators of thermal maturity including organic, geochemical, mineralogical and thermochronometric parameters are in use. Thermochronological techniques (e.g. apatite fission track analysis and diffusion of helium during U-Th decay) are commonly used for assessing the maximum paleotemperatures and timing of thermal events in an area; however, vitrinite reflectance is one of the least expensive and most widely used organic indicator of thermal maturity (Japsen et al., 2007; Green et al., 2017; Nielsen et al., 2017). The vitrinite reflectance is useful over a wide range of maturation and is particularly useful in the maturation range of interest in exploration for hydrocarbons (Nielsen et al., 2017).

The vitrinite reflectance is directly dependent on temperature and residence time and provides useful information on the thermal history of the basin (Dow, 1977; Waples, 1980a; Lerche et al., 1984; Cope, 1986; Mukhopadhyay and Dow, 1994). The vitrinite reflectance is largely considered an irreversible parameter (Cope, 1986). The reflectance of organic matter increases with increasing temperature and freezes with decreasing temperature, indicating maximum temperature to which the sediments were exposed to during their burial history (Waples, 1980a; Middleton, 1982; Archard et al., 1998). Analysis of available vitrinite reflectance data, therefore, can provide an estimation of the amount of missing sedimentary sections through examination of thermal maturity profiles.

The measured vitrinite reflectance data compiled from exploration borehole's geochemistry reports were plotted against depth below seafloor on a semi-logarithmic scale. The best-fit regression lines were drawn and extrapolated to near-surface values of 0.2% (Sweeney and

Burnham, 1990). The difference between the seabed and extrapolated depth at vitrinite reflectance value of 0.2% was then estimated as net uplift/erosion (Fig. 4).

The vitrinite reflectance method was originally designed for rank determinations on coals but later extended to finely disseminated organic material in clastic sediments (Hacquebard and Donaldson, 1970). This extension, however, introduced certain limitations which is essential to be aware of when interpreting vitrinite reflectance data obtained from clastic sediments. Reliable and readily interpreted vitrinite reflectance data are relatively rare, poor and even barren samples are very frequent. This is due to a number of factors including type of lithology selected for study, small particle size, poor particle quality, bitumen staining, low reflecting vitrinite, weathering, lack of vitrinite, difficult identification of vitrinite, reworked and/or oxidized vitrinite, other macerals with higher reflectivity like inertinite, high pyrite contents and cavings (Tissot et al., 1987; Mukhopadhyay, 1992; Mukhopadhyay and Dow, 1994; Suggate, 1998). Therefore, when constructing best-fit regression lines, preference (in order from high to low) was given to the data points from coal samples; kerogen concentrated conventional core and sidewall core samples; and bulk rock samples with a high population of mean vitrinite reflectance.

It is also vital to consider geothermal gradient while constructing best-fit regression lines (Waples, 1980b). Vitrinite reflectance is highly sensitive to the temperature gradient and relatively less sensitive to the time spent. Vitrinite reflectance increases with increasing geothermal gradient. Therefore similar geothermal gradients are expected to show similar vitrinite reflectance depth trends. However, this may not be the case if sedimentation or heating rates are different (Suggate, 1998). Present-day heat flow and geothermal gradients are varying throughout the North Sea Basin, therefore, rather than using an average geothermal gradient curve for the entire Norwegian North Sea Basin, a series of vitrinite reflectance versus depth curves were calculated based on the Sweeney and Burnham (1990) algorithm for different geothermal gradients by assuming a continuous burial/subsidence and constant heating rates of 1 °C/Ma (Fig. 4). Any change in the present-day temperature gradient from the paleotemperature gradient will give rise to an uncertainty in the exhumation estimates. For example, a 1 °C/km change in temperature gradient will give an uncertainty of ±100 m in exhumation estimates. In general, uncertainty regarding exhumation estimates from vitrinite reflectance data is more than approximately ±200 m due to its semi-logarithmic relationship with the depth and high sensitivity to changes in the geothermal gradients.

4. Results

This section summarizes the results from the sonic log and vitrinite reflectance data and uses these results to model 1-D isostatic compensation of the lithosphere due to the removal of the overburden and investigate the paleogeography of the areas before the onset of uplift and erosion. The data coverage was generally good in most of the Norwegian sector except on the platform areas (e.g. in the Stavanger Platform and Horda Platform areas in Fig. 2). Therefore, additional data constraints for better boundary conditions were added from exhumation estimates along transect-2 in Fig. 2, and Figures 4 and 5 in Riis (1996). The exhumation along these sections was estimated by extrapolating the basin stratigraphy into the basin margin areas. In addition to available sonic log and vitrinite reflectance data, exhumation estimates from interval velocities from check shot data compiled from Nielsen and Japsen (1991) were included for increasing the data density in the Danish sector (Fig. 5a). As stated in the methodology section, different sets of reference compaction curves were established for different lithostratigraphic units. Therefore, the resulting map presented in Fig. 5a, is thus arithmetic mean of exhumation estimated from Early Cretaceous -Early Miocene shales and Late Cretaceous-Early Paleocene chalk penetrated in a single borehole.

4.1. Exhumation estimates from compaction and thermal maturity techniques

Exhumation maps presented in this study are based on observed data but have some limitations regarding data consistency/availability and choice of methods applied. Exhumation maps are spatially better constrained from compaction technique due to the availability of sonic log data in a large number of boreholes as compared to thermal maturity data (Fig. 2). However, exhumation maps from both compaction and thermal maturity techniques may be somewhat uncertain within the Farsund Basin, Stavanger Platform and southern part of Stord Basin area and towards the Norwegian coast due to poor data coverage and extrapolation of trends towards the edges of the study area (Fig. 5a-d). Exhumation maps were computed in Petrel software for both the compaction and thermal maturity techniques but since thermal maturity data lacked control points in the southeastern part of the study area, therefore in this part of the study area, contour lines for the thermal maturity results were computed using boundary conditions (towards edges) from the compaction technique results. In figure 6c, a difference between exhumation estimates from compaction techniques and thermal maturity techniques is shown to highlight the differences in results from each method. Also, arithmetic mean of net exhumation from both datasets was calculated to minimize over- and/or under-estimations related to any particular technique (Fig. 5d).

The exhumation estimates from compaction techniques and thermal maturity techniques complement each other reasonably well, and the difference is generally less than ±200 m throughout the study area. The exhumation estimates roughly follow the north-south trend and increase towards the east (Fig. 5). Sonic velocity and vitrinite reflectance analysis suggest that widespread exhumation has occurred in the basin margin areas, towards the east, both in the Norwegian and Danish sectors. Average net exhumation estimates range from minor or no exhumation in the Central Graben and south Viking Graben areas to >1100 m towards the Norwegian coast.

4.1.1. Central and eastern North Sea

A large number of boreholes are drilled in the Central Graben basin area, and sonic log data from selected boreholes were used to establish normal compaction curves for different lithostratigraphic units in the central North Sea area (Fig. 2). Exhumation estimates from sonic logs and vitrinite reflectance data indicate that all lithostratigraphic units are currently at their maximum burial depth within the Central Graben basin area, whereas exhumation estimates in the flanking areas (e.g. Jæren High and Sørvestlandet High in Fig. 2) vary from no exhumation in western parts to minor exhumation (<100 m) in eastern parts (Fig. 5). Average exhumation estimates within the Ringkøben-Fyn High area are increasing towards the east and vary from no exhumation in the western part to ~300 m of exhumation in the eastern part (Fig. 5d).

No deep well is drilled in the Norwegian sector except a couple of shallow boreholes drilled within the Norwegian Channel in the northern part of the Sorgenfrei-Tornquist Zone area (e.g. 13/1-U-1 in Fig. 2). Upper Jurassic shales were penetrated directly below the Quaternary sediments in one of the shallow borehole 13/1-U-1, and sonic velocity data from this borehole was used to constraint the exhumation estimates towards the northern part of the Sorgenfrei-Tornquist Zone. The sonic velocity data from two offshore and three onshore boreholes in the Danish sector were also utilized to map the distribution of net exhumation in this area (Fig. 5a). The vitrinite reflectance data from two boreholes in the Danish sector were compiled from Japsen et al. (2007) (Fig. 2 and Fig. 5b). The results indicate that exhumation magnitudes are increasing towards the north and east. Exhumation estimates from both sonic velocity and vitrinite reflectance data are ≥ 900 m within the Sorgenfrei-Tornquist Zone area, ≥ 1300 m to the north in the shallow borehole in the Norwegian sector and ≥ 800 m in the Danish sector to the southeast (Fig. 5a-b).

Norwegian-Danish Basin covers a large area both in the Norwegian and Danish sectors. Data coverage is relatively good (Fig. 2). The exhumation estimates are based on the analysis of sonic velocity data from nearly 20 boreholes in each of the Norwegian and Danish sectors together with the analysis of vitrinite reflectance data from 8 and three boreholes, respectively, in the Norwegian and Danish sectors. Vitrinite reflectance data were compiled from Japsen et al. (2007) in the Danish sector (Fig. 2). Average exhumation estimates are increasing towards north and northeast and vary from ~400 m in the south to ~800 m in the north and east in the Danish sector (Fig. 5d). Exhumation magnitudes are increasing towards northeast within the Norwegian sector. Average exhumation estimates vary from <300 m in the west and northwest to >800 m towards the east (Fig. 5d).

Data coverage in the Egersund Basin area is good. Exhumation estimates are based on analyses of sonic log and vitrinite reflectance data in 18 and 12 boreholes, respectively (Fig. 2). Average exhumation within the Egersund Basin roughly follows the N-S trend and increases to the east (Fig. 5d). Average exhumation varies from ~200 m in the west to ≥ 600 m in the east. Exhumation increases to the North and roughly follows the E-W trend within the Lista Fault Blocks. Exhumation estimate varies from ~500 m in the south to ~700 m in the north (Fig. 5d). Average exhumation estimated from both sonic logs and vitrinite reflectance data is ≥ 600 m from a single borehole drilled in the Stavanger Platform area. The exhumation estimates along a depth converted seismic geo-section from Riis (1996) were also incorporated in the Stavanger Platform area to restrict the exhumation estimates towards the edges of the study area (Fig. 5a). The average exhumation map shows that exhumation estimates are increasing towards north-northeast and varying from ~600 m towards the west to ~1100 m towards the north in the Stavanger Platform area. Exhumation estimates from sonic log data indicate ≥ 800 m of the missing section in a single borehole located on the southern flank of the Farsund Basin area and ≥ 700 m in a borehole located in the Fjerritslev Trough area (Fig. 5a).

Sonic log data from six boreholes and vitrinite reflectance data from four boreholes were analysed in the Sele High, Åsta Graben, and Ling Depression areas (Fig. 2). Average exhumation estimates are increasing towards the east in this area and vary from <200 m towards west to <400 m towards east in the Sele High area, no exhumation towards southwest to > 600 m towards northeast in the Ling Depression area and ~400 m to ~900 m in the Åsta Graben area (Fig. 5).

4.1.2. Northern North Sea

The majority of well logs used to establish normal compaction curves in the northern North Sea were located in the south Viking Graben area (Fig. 2). The results indicate that all lithostratigraphic units are currently at their maximum burial depth in the south Viking Graben area. Results from sonic log data from nearly 20 boreholes and vitrinite reflectance data from six boreholes indicate minor (<100 m) or no exhumation in the Utsira High area (Fig. 5).

The well data coverage is poor towards the south of the Troll Field in the Stord Basin area where data from only three exploration boreholes drilled on the southwestern margin were analysed (Fig. 2). Therefore, exhumation estimated along two depth converted seismic sections (one from Riis (1996) and the other from First Geo, transect-2 in Fig. 2) were also included in the final results to increase the data resolution in the Horda Platform area. Analyses of sonic log and vitrinite reflectance data and seismic stratigraphy in the area suggest that significant exhumation must have taken place in the area. Average exhumation estimates are increasing from west to east and varying from <100 m to >700 m in the southern part and about 200 to 900 m in the northern part of the Stord Basin area (Fig. 5d). Results from sonic log data from two boreholes and vitrinite reflectance data from one borehole in the Patch Bank Ridge area also indicate increasing exhumation magnitudes towards the east and vary from about <100 m in the western parts to ~500 m in the eastern parts (Fig. 5d).

Vitrinite reflectance and sonic log data from a large number of boreholes were analysed in the north Viking Graben area (Fig. 2). Results indicate minor or no exhumation in the west and increasing exhumation to the east. The exhumation estimates differ significantly for areas outside and inside the Norwegian Channel in the northern North Sea area. Average exhumation is usually ≤100 m outside the Norwegian Channel but varying from about 200 m to ≥ 800 m in the areas within the Norwegian Channel (Fig. 5d). Average exhumation varies from <100 m to the southwest and up to ~400 m to the northeast within the north Viking Graben area. No to minor exhumation (<200 m) is estimated within the Tampen Spur area. The exhumation estimates vary from <400 m to <800 m on the sloping terraces towards east (Fig. 2 & 5d).

4.2. Isostatic response to erosion and deposition of sediments

Isostatic models suggest that any topographical load regardless of their size, are compensated locally, and isostasy is achieved either by laterally varying thickness of a crust of uniform density (Airy model) or by lateral changes in density of a uniform thickness crust (Pratt model) or by some combination of these factors (Watts, 2001). Isostatic rebound occurs when a load is added or removed from the crust. Simple Airy isostasy modelling indicate that isostatic rebound is mainly a function of isostatic compensation (i) and thickness of load (h_l) added or eroded from the top of the crust (Eq. 10). The isostatic compensation is the ratio of the density of the material (ρ_c) added or eroded from the top of the crust and the density of the mantle (ρ_m) at a depth of compensation (Gilchrist et al., 1994).

$$Isostatic\ rebound = \frac{\rho_c}{\rho_m} * h_l \qquad Eq.\ 10$$

In this study, the airy isostasy model is used which is very often used in basin modelling programs to calculate isostatic rebound. The objective of the modelling is to estimate the magnitude of isostatic readjustment resulting from the removal of sediments and/or increased water/sediment load and the changes in elevation after isostatic equilibrium is reached. This would help to configure ground elevation conditions before the start of erosion. The current study indicates that more than 1 km sediments are eroded in the North Sea basin margin areas (Fig. 5) and additional water/sediment load may also have influenced isostatic adjustment in the area (Eqs. 11 and 12). Based on analysis of bulk density logs, the density of the sediments (ρ_{sed}) eroded is varying between about 2.1–2.3 g/cm^3 in the area. The density of mantle and water are assumed to be 3.3 g/cm^{3}and ~1.0 g/cm^3, respectively. Isostatic uplift due to the erosion of sediments (Fig. 6a) and isostatic subsidence due to increase in the water/sediment load (Fig. 6b) was calculated using the thickness of eroded sediments (h_e) and water depths (h_w), respectively (Eqs. 11 and 12). Assuming that isostatic equilibrium is regained in the area, about 60–70% of the surface elevation reduced by erosion may have been restored by isostatic uplift (Fig. 6a).

$$Isostatic\ uplift = \frac{\rho_{sed}}{\rho_m} * h_e \qquad Eq.\ 11$$

$$Isostatic\ subsidence = \frac{\rho_w}{\rho_m} * h_w \qquad Eq.\ 12$$

In the modelling it is assumed that sea level was close to zero before the start of erosion and that the additional water load may have caused isostatic subsidence and further lowering of the surface elevation (Fig. 6b). Assuming that there is no additional tectonic uplift/subsidence and isostatic equilibrium is regained, change in the surface elevation of the crust from its original position before the erosion took place will be the difference between exhumation estimates and isostatic rebound (Eq. 13 and Fig. 6c).

$$Change\ in\ surface\ elevation = net\ exhumation - (isostatic\ uplift - isostatic\ subsidence) \qquad Eq.\ 13$$

The map shown in Fig. 6c indicates that the maximum change in surface elevation may have occurred within the Norwegian Channel along the southwest coast of Norway and present-day surface elevation may be between about 400–700 m lower than its original position before the erosion took place. Similarly, the present-day surface elevation in the Norwegian-Danish Basin area may be about 350 m lower than its original position. The present-day surface elevation of the crust which is the result of erosion of the sediments and isostatic rebound in the area can be restored to its original position before the erosion took place by Eq. 14 (Fig. 6d).

$$Paleosurface\ elevation = total\ change\ in\ elevation + present\ surface\ elevation \qquad Eq.\ 14$$

Restoring the present-day surface elevation to the original position before the erosion took place indicates exposed areas in the Norwegian-Danish Basin and along the southwest coast of Norway (Fig. 6d). The map indicates that the Norwegian-Danish Basin area may have been around 200-300 m above sea level before erosion took place leaving the area exposed to subaerial processes. Similarly, the map also identifies exposed areas under the Norwegian Channel and along the southwest coast of Norway.

5. Discussion

This section compares the results from the current study with the published work and discusses the significance of the results in the area. The results from different lithostratigraphic units are also compared to discuss the relevance to the timing of uplift and erosion. In the last part, the implications of exhumation are discussed for predicting the rock properties and its effects on the seal and source rock properties in the central and northern North Sea.

5.1. Comparison with published studies

Many authors have used compaction and thermal maturity based techniques similar to current study to estimate exhumation along the North Sea Basin margin areas particularly during the 1990s (e.g. Ghazi, 1992; Jensen and Schmidt, 1992; Hillis, 1995; Doré and Jensen, 1996; Hansen, 1996; Riis, 1996; Japsen, 1998; Huuse, 2002; Japsen et al., 2007; Japsen et al., 2008). The exhumation estimates from the current study are compared with these previously published studies. For this purpose, four studies were selected, and exhumation maps were digitized and imported into the Petrel software. Two out of these four studies were focused mainly in the central and eastern North Sea (Jensen and Schmidt (1992), Japsen (1998)), whereas the other two (Doré and Jensen (1996), Riis (1996)) give good coverage along entire offshore Norway. The methodology behind the exhumation maps of Jensen and Schmidt (1992) and Japsen (1998) was based on shale/chalk compaction and vitrinite reflectance analyses of boreholes similar to the current study. Doré and Jensen (1996) also used well data from approximately 200 boreholes along entire offshore Norway. Their exhumation map was based on estimates from the well data and graphical reconstruction of onshore topography. The source of the exhumation map of Riis (1996) was based on structural reconstruction and extrapolation of offshore/onshore geology.

All four studies show that exhumation estimates are increasing towards the Norwegian coast, but exhumation magnitudes may vary between each study. The boundary between exhumation and no exhumation areas runs through the middle of the Norwegian-Danish Basin in Jensen and Schmidt (1992), Riis (1996) and Japsen (1998), whereas through the middle of the Egersund Basin in Doré and Jensen (1996). Jensen and Schmidt (1992), Doré and Jensen (1996) and Japsen (1998) estimated <500 m, Riis (1996) estimated <300 m of uplift and erosion in the Egersund Basin area. A significant uplift and erosion (> 700 m) is documented in the Stavanger Platform area by all four studies. In the Skagerrak area, Jensen and Schmidt

(1992), Doré and Jensen (1996) and Riis (1996) estimated more than 1100 m of uplift and erosion, whereas Japsen (1998) estimated up to 900 m of uplift in the same area.

The exhumation estimates from the current study are compared with the published studies along three depth-converted seismic transects in the central and northern North Sea (Fig. 2). Transect-3 is oriented NE-SW and passes through the Central Graben, Sørvestlandet High, Norwegian-Danish Basin, Egersund Basin to the Stavanger Platform. All units are shallowing up towards NE and truncated below the mid-late Quaternary unconformity towards the coast (Fig. 7a). Considerably thick (up to 3000 m) Nordland Group and Hordaland Group sediments are present in the Central Graben and are thinning towards the coast. The Nordland and Hordaland Group sediments are completely eroded below the mid-late Quaternary unconformity within the Egersund Basin, and further to the east in the Stavanger Platform area, respectively. All four studies show no exhumation in the Central Graben or Sørvestlandet High areas. Exhumation estimates are increasing towards NE and vary from 0-800 m from Jensen and Schmidt (1992) and Doré and Jensen (1996), 0-700 m from the current study, 0-300 m from Riis (1996) and 0-500 m from Japsen (1998) along the transect-3. Comparison of exhumation estimates along transect-3 from these studies is presented in Table 2.

Seismic transect-2 is also oriented NE-SW and passes through south Viking Graben, northern part of Utsira High and Stord Basin to the Øygarden Fault Complex (Fig. 2). No exhumation is shown in any of the wells along this transect, but exhumation is increasing from east of well 26/4-1 towards the coast where Jurassic to early Quaternary strata is truncated below the angular unconformity at the base of Norwegian Channel (Fig. 7b). Exhumations estimates vary from 0-900 m from the current study, 0-1000 m from Doré and Jensen (1996) and 0-550 m from Riis (1996).

Seismic transect-1 is oriented WNW-ESE and passes through north Viking Graben to the northern part of Stord Basin (Fig. 2). Exhumation estimates vary from 0-1000 m from the current study, 0-800 m from Doré and Jensen (1996) and 0-550 m from Riis (1996) (Fig. 7c). The exhumation estimates from the current study and Doré and Jensen (1996) and Riis (1996) are significantly different along the transect-1. For example, the current study suggests that more than ~350 m sediments are eroded in wells 31/2-15 and 31/2-6, but both Doré and Jensen (1996) and Riis (1996) maps show no exhumation in areas near these wells. Similarly more than ~900 m sediments are eroded in well 32/2-1 but Doré and Jensen (1996) estimated 470 m of exhumation and Riis (1996) estimated about 390 m of exhumation. The results from the current study are further supported by the seismic data which show that Early Cretaceous Cromer Knoll Group is partially eroded below the angular unconformity, but thick sediments of Paleocene- Eocene Rogaland Group, Eocene-Early Miocene Hordaland Group are completely eroded at well 32/2-1 (Fig. 7c). Comparison of exhumation estimates along transect-3 is given in Table 3.

Vertical and lateral velocity variation plots through Eocene-Early Miocene Hordaland shales, Paleocene- Eocene Rogaland shales, Late Cretaceous-Early Paleocene Shetland shales/carbonates, and Early Cretaceous Cromer Knoll shales along the three transects are also included in the Appendix-1.

5.2. Comparison of exhumation estimates from shales and carbonates

Different sets of normal compaction curves established for different lithostratigraphic units were used to estimate exhumation in the basin margin areas (Fig. 3c). Exhumation estimates from carbonates and shales in the Shetland Group were particularly compared with estimates from shales of the Hordaland and Cromer Knoll groups in the central and northern North Sea (e.g. Table 1). A strong correlation between exhumation estimates from different stratigraphic units was observed throughout the study area (Fig. 8). The similarity of results from the Early

Cretaceous to Early Miocene sediments suggests that maximum burial may have been reached sometime after the Early Miocene in most of the areas. Figure 1 shows that Lower Quaternary strata are subcropping below the mid-late Quaternary unconformity in the Egersund Basin and Ling Depression areas. Furthermore, graphical reconstruction of seismic stratigraphy indicates that considerable sediments (up to 600 m) must have been deposited during the Early Quaternary in these areas before these were later eroded below the mid-late Quaternary unconformity (Baig, 2018).

5.3. Timing of uplift and erosion

5.3.1. Central and eastern North Sea

Cretaceous to Early Quaternary strata are subcropping below mid-late Quaternary glacial sediments in the Norwegian-Danish Basin area and the basin margin areas further east (Fig. 1). This unconformity has been developed as a result of repeated shelf edge glaciations of the area during the last ~0.45 Myr (Cameron et al., 1987; Jansen and Sjøholm, 1991; Stoker et al., 1994; Eidvin et al., 2000; Dahlgren et al., 2002; Sejrup et al., 2005; Nielsen et al., 2008; Lee et al., 2012). The results from this study indicate that about 200 to 1000 m sediments are eroded below this unconformity (Fig. 1 and Fig. 5). Apatite fission track analysis (AFTA) data suggested that the North Sea area has been affected by mainly two major uplift and erosion episodes during the Cenozoic time. The first phase of uplift and erosion was linked with the uplift and erosion of the Scandinavia, and it affected mainly the eastern North Sea (Rohrman et al., 1995; Riis, 1996; Kyrkjebø et al., 2000; Faleide et al., 2002; Japsen et al., 2007). This is indicated by unconformities at the base and top of Oligocene in the eastern North Sea areas (Japsen et al., 2007). Late Neogene exhumation affected the entire Norwegian Continental Shelf including the North Sea, Norwegian Sea and Barents Sea (Doré and Jensen, 1996; Japsen et al., 2007; Anell et al., 2009; Baig et al., 2016). Large thickness of early Quaternary sediments indicates subsidence of the deep basin areas, whereas regional unconformities at the base and top of early Quaternary succession indicate tilting of the hinterland areas in the central and northern North Sea (Japsen et al., 2007; Baig, 2018). It is, however, unclear if tilting of the basin margin areas led to subsidence in the deep basin areas or vice versa. The AFTA data indicated that exhumation of the hinterland areas might have started ~4 Ma and continued during the regional tilting taking place at the beginning of the Quaternary period (Rasmussen et al., 2005; Japsen et al., 2007).

It is important to know if tilting of the basin margin areas also continued in the Miocene-Pliocene period and to what extent it has affected the deep basin areas since the uplift and erosion of mainland southern Norway during the Oligocene. Another critical question relates to whether all the sediments in the basin margin areas were eroded due to mid-late Quaternary glacial processes exclusively or if there was any erosion occurred during the Miocene-Pliocene period. Resolving this matter will help to configure burial and exhumation histories of the basin margin. For this reason, the sedimentary record preserved in the deep basin areas was extended into the basin margin areas. Figure 9 shows a WSW-ENE oriented seismic section through two boreholes Inez-1 and Felicia-1, located about 105 km apart, in the Norwegian-Danish Basin and Sorgenfrei-Tornquist zone areas, respectively. Top of Chalk Group is marked at 800 mbsf in borehole Inez-1 and 45 mbsf in Felicia-1 (Nielsen and Japsen, 1991). Chalk Group sediments are overlaid by Hordaland Group in Inez-1 and shallowing towards the east and truncated below mid-late Quaternary sediments in Felicia-1. The Chalk Group is about 425 m and 600 m thick in Inez-1 and Felicia-1 boreholes, respectively. The thickness of Chalk Group is increasing towards the east, and a maximum thickness of about 1100 m is estimated using interval velocity of 3400 m/s somewhere between Inez-1 and Felicia-1 before it is truncated below the mid-late Quaternary sediments to the east (Fig. 9). The overlying Oligocene sediments are more than about 400 m thick in the Inez-1 and thinning towards the east in contrary to the Chalk Group before these are completely eroded in the Felicia-1. By extending these sequences to the east, it showed that the top of Upper Oligocene strata might be truncating/onlapping the Lower Oligocene strata to the east of Inez-1 indicating areas of negative accommodation/topography further east in the Sorgenfrei-Tornquist Zone area (Fig. 9). It indicates that more than about 800-900 m sediments including from the lower part of the Hordaland and the upper part of Shetland groups may have been eroded during the Late Oligocene in Felicia-1 (Fig. 10a). A shallow basin existed afterward, and about 300-500 m sediments may have been deposited later during the Miocene-Pliocene in the Norwegian-Danish Basin and Sorgenfrei-Tornquist Zone areas between the Felicia-1 and Inez-1 boreholes, which were also eroded later during the late Neogene. This indicates that the magnitudes of Late Oligocene uplift and erosion were more than the magnitudes of uplift and erosion during the late Neogene and that the maximum burial may have been reached before the Late Oligocene in the Sorgenfrei-Tornquist Zone area (Fig. 10a). However, further to the west, for example in Inez-1 well the thickness of Miocene-Pleistocene sediments was large enough to mask effects of the erosion (if any) of sediments during the Late Oligocene event in the Norwegian-Danish Basin indicating that maximum burial may have been reached during the Miocene-Pliocene or even during Pleistocene (Fig. 10b). The timing of maximum burial sometime during the Oligocene in the Sorgenfrei-Tornquist Zone area also correlates closely with the onset of cooling during 30-20 Ma obtained from AFTA data in Felicia-1 well by Japsen et al. (2007). Our exhumation estimates of 900 m for the Felicia-1 well are also in agreement with the estimates of Japsen et al. (2007) (800-1000 m) and Jensen and Schmidt (1992) (1000 m). However, Jensen and Schmidt (1992) exhumation estimates (1000 m) for the Inez-1 well are a bit too higher than from the current study (620 m) and Japsen (1998) (655 m).

Further to the northwest of Felicia-1 well, Japsen et al. (2010) estimated about 500 m of net exhumation in the Ling Depression area in well 17/3-1. They proposed that the maximum burial in this area took place in the early Miocene before the mid-Miocene hiatus. The current study also indicates that about 670 m (570 m net exhumation +100 m mid-late Quaternary reburial) sediments have been eroded below the angular unconformity. Study of Quaternary sediment distribution shows that a major early Quaternary system was prograding to the west-northwest in this area (Baig, 2018). However, the early Quaternary sediments are eroded below the angular unconformity near the 17/3-1 well. Reconstruction of the seismic stratigraphy suggests that more than ~600 m of early Quaternary sediments must have been deposited in this area before these were completely eroded below the angular unconformity indicating the timing of maximum burial most likely in the early Quaternary. The Cenozoic burial history of sediments at 17/3-1 well location is discussed in detail in section 5.6.

Same is the case in the Egersund Basin area and northwestern part of the Norwegian-Danish Basin where analysis of seismic sequences also indicates that significant early Quaternary sediments have been eroded below the mid-late Quaternary unconformity and the maximum burial may have been reached most likely sometime during the early Quaternary. Study of seismic sequences also indicates that coastal and/or deltaic environments were dominant on the basin margin areas and migrated to west-northwest during the early Quaternary in the central North Sea (Baig, 2018). This suggests that there is a possibility that sediments on the basin margin areas to the east were removed and redeposited in the adjacent deep basin to the west-northwest. Removal of sediments from the overburden will cause isostatic uplift of the ground to achieve isostatic balance. Reconstruction of paleo-surface elevation to its original position before the erosion took place and its comparison to offlap break positions indicates that the Egersund Basin area and the Norwegian part of the Norwegian-Danish Basin may have been subaerially exposed by the end of the early Quaternary (Fig. 11). Late Neogene uplift and erosion may be diachronous in the eastern and central North Sea so that areas to the east in the Danish part of the Norwegian-Danish Basin may have been subaerially exposed even earlier about at 4 Ma (Japsen et al., 2007).

5.3.2. Northern North Sea

The timing of uplift and erosion in the northern North Sea can be rather well constrained from the pre-Quaternary depositional and subcrop patterns compared to in the central and eastern North Sea. The pre-Quaternary deposition in the northern North Sea Basin was mainly a response to sea-level fluctuations during Paleocene to Pliocene and depositional styles are characterized by superimposed depocentres and eastward progradation of sediments in the Viking Graben area sourced mainly from the East Shetland Platform (Faleide et al., 2002; Anell et al., 2012; Jarsve et al., 2014b). A major shift in sediment source in the northern North Sea area occurred at the beginning of the early Quaternary when southern Norway took over from the East Shetland Platform as the main sediment source area (Anell et al., 2012; King, 2016; Baig, 2018).

Thick wedges of early Quaternary sediments were deposited directly above the mid-Miocene seismic unconformity (MMU) in the Stord Basin and north Viking Graben areas (Baig, 2018). This indicates uplift and erosion of southern Norway sometime during the late Neogene and subsequent filling of the newly created accommodation and westward progradation of the sediments derived from southern Norway. The top parts of the early Quaternary prograding wedges are also eroded below the angular unconformity at the base of the Norwegian Channel indicating that the latest phase of erosion took place after the deposition of the early Quaternary prograding wedges in the northern North Sea. The oldest till units studied in the Norwegian Channel suggest glaciogenic growth of the huge North Sea Fan since at least about 1.1 Ma implying a glacial environment along the southwest coast of Norway (Sejrup, 1995). The fast-moving ice streams eroded a trough between 200 and 600 m deep in the early

Quaternary down to the Cretaceous strata. This indicates that most of the eroded material from the onshore and the coastal areas of southern Norway may have been transported along the Norwegian Channel by subglacial processes and deposited in the huge North Sea Fan at the mouth of the Norwegian Channel. The results from this study indicate between 200 and 1100 m of net exhumation below the angular unconformity in the northern North Sea. The thickness of post exhumation sediments above the angular unconformity is about 200 m which indicate that between 400 to 1400 m of sediments must have been eroded below the angular unconformity.

5.4. Shale compaction and paleotemperature

Mechanical compaction in siliciclastic sediments due to the weight of overburden sediments is dominant at shallow burial depths <2 km and temperature < 70-80 °C. Transformation of smectite to illite is the most important chemical process at temperatures more than 70–80 °C (Bjørlykke and Høeg, 1997; Bjørlykke, 1998). This temperature range is also related to the onset of quartz cementation in sandstones (Thyberg et al., 2010; Thyberg and Jahren, 2011). Depending on mineralogy and mineral transformation reactions, cementation may have a significant effect on shale properties and it may change the shale rheology from more ductile (softer rock, self-healing low conductivity cracks) in the mechanical compaction domain to more brittle (stronger rock, high conductivity cracks) in the chemical compaction domain (Dewhurst and Jones, 2002).

Average shale velocities observed within the Nordland Group range from ~1700 to 1900 m/s in wells 7/1-1, 7/3-1, 8/1-1, 8/3-1, 8/3-2 and 9/2-2, whereas average shale velocities within the Hordaland Group range from ~1900 to 2100 m/s in wells 6/3-2, 7/1-1, 7/3-1, 8/1-1, 8/3-1, 8/3-2, 9/2-2 and 9/3-1 (Fig. 12a-b). The low and narrow range of shale velocities observed in the Nordland and Hordaland groups indicate probable mechanical compaction of the sediments. The analyses of thermal maturity data also indicate that sediments of the Nordland and

Hordaland groups may have never been buried deep enough to be chemically compacted. Intermediate range and spread of shale velocities (2000–2500 m/s) observed within the Rogaland Group in blocks 6/3-2, 7/3-1, 8/1-1, 8/3-1, 8/3-2, 9/2-1, 9/2-2 and 9/3-1, may indicate the onset of chemical compaction in the central North Sea. Average shale velocities observed within the Cromer Knoll Group range from 2200 to 3200 m/s in blocks 7/1-1, 7/3-1, 8/1-1, 8/3-1, 8/3-2, 9/2-1, 9/2-2, 9/2-3. 9/2-5, 9/2-7S and 9/3-1, and within the Viking Group velocities range from 2500 to 3400 m/s in blocks 7/3-1, 8/1-1, 8/3-1, 9/2-1, 9/2-2, 9/2-3, 9/2-5, 9/2-7S and 9/3. The higher and wider range of velocities in shales of the Cromer Knoll and Viking groups indicate dominant chemical compaction of these sediments (Fig. 12d).

Assuming an average geothermal gradient of ~35 °C/km in the North Sea Basin would suggest that the onset of chemical compaction should occur at burial depths deeper than 2 km (Bjørlykke, 2014). Transition zones between the mechanical and chemical compaction domains were identified in each borehole based on velocity-depth, and velocity-porosity relationships. The onset of chemical compaction in areas of minor exhumation (<100 m) or currently at their maximum burial is mainly observed at the base of the Hordaland Group or within the Rogaland Group at > 2 km present-day burial depths (Fig. 12). Analyses of thermal maturity and well log data in the basin margin areas to the east indicate higher thermal maturity and geophysical properties (density and velocity) corresponding to deeper burial depths and the onset of chemical compaction may be located within the carbonates of the Shetland Group at present-day burial depths of less than 1.2 km. The boreholes, currently not at their maximum burial depth, show significantly lower present-day temperature within the transition zones due to the exhumation. For example, Fig. 13 shows an example of present-day temperature through an exhumed (17/3-1) and unexhumed well (2/7-2). The transition zone is probably located at 2.3 km in the unexhumed well, and the present-day temperature is between 70-80 °C at this depth. The likely transition zone is located between 1-1.2 km in the exhumed well, whereas present-day temperature is less than 60 °C at this depth indicating colder temperature. Paleotemperatures were derived from vitrinite reflectance data using the algorithms given in by Barker and Pawlewicz (1994) and (Corcoran and Clayton, 1999) (Eqs. 15 & 16). This may help to indicate maximum temperatures to which these sediments were exposed before uplift and erosion (Fig. 13). The vitrinite reflectance derived temperatures indicate that sediments at the observed transition zone may have been exposed to hotter temperatures (70-80 °C) in the exhumed well.

$$Tmax = \frac{(lnRo+1.68)}{0.0124} \qquad Eq.\ 15$$

$$Tmax = \frac{(lnRo+1.4)}{0.0096} \qquad Eq.\ 16$$

Bottom hole temperature (BHT) data was acquired from Norwegian Petroleum Directorate (2018), and all BHT data is Horner corrected. For consistency purposes, only those wells are used for calculating the present-day geothermal gradients where total depth (TD) is more than 2 km (Fig. 14a). The onset of chemical compaction identified from a combination of velocity-depth and velocity-porosity relationships was used as input to map the areal distribution of the present-day depth at the observed transition between the mechanical and chemical compaction, and its relationship with the present-day temperature at this depth (Fig. 14b). The depth at which the transition between mechanical and chemical compaction occurs, together with the geothermal gradient, help us to separate areas where shales have ductile rheology from those where stiffening by quartz cementation may yield brittle rheology (Fig. 14b). This has direct implications for seal integrity for CO_2 storage in these areas. The depth of transition between mechanical and chemical compaction is an indirect indicator of the rheology of shales. Shales are expected to behave more ductile at depths shallower than the transition zone and will behave more brittle at depths deeper than the transition zone (Fig. 14b).

5.5. Implications for seal rock properties

Understanding the rheological changes of seal rocks is important for both hydrocarbon and CO_2 storage/leakage viewpoints (Angeli et al., 2013). Comparison of horizontal stresses obtained from leak off tests in exhumed and non-exhumed areas indicates reduced horizontal stresses in the sediments, which are currently not at their maximum burial depth (Fig. 15). It is of particular interest that the reduction in minimum horizontal stresses is found at deeper depths (> 1.5 km). The differences seen in minimum horizontal stresses at shallow depths were much smaller. This may be due to the effect of increased chemical compaction and brittleness of shales buried to greater depths resulting in possible fracturing during uplift and erosion in response to unloading. These observations also suggest a direct relationship between brittleness and chemical compaction of clays. The effect of cementation on the relationship between horizontal and vertical effective stresses in clays was also observed by Berre et al. (1995) and Nygård et al. (2004). They observed that the ratio between horizontal and vertical effective stresses is decreased during unloading in cemented clays in contrast to the typically increased values in uncemented clays or shales. The decreased ratio between horizontal and vertical effective stresses will have important implications on possible hydraulic fracturing pressures in cemented sediments in the study area. When cemented shales are uplifted and effective vertical stress is decreased then shales enter into a strength field in which brittle fracture dominates at lower strain levels. This means that it is easier to hydraulically fracture cemented shales than shales which have only been mechanically compacted to the same vertical stress level (Hoshino et al., 1972; Sales, 1993; Nygård et al., 2004; Kalani et al., 2015). Transient overpressure in shales in addition to reduced confining pressure by unloading may also cause hydraulic fracturing. Fracturing and seal failure may also increase at the boundary between areas of differential uplift/subsidence or by later tectonic activity (Sales, 1993; Kalani et al., 2015).

High horizontal stresses towards the west and decreasing horizontal stresses to the east towards the coast in the north Viking Graben area were also observed at depths greater than 1.5 km by Grollimund and Zoback (2000). It was interpreted as an effect of the flexural response of crust to thick ice loading towards the coast. Based on the results of analytical and mathematical modelling of plate flexure they suggested that the observed lateral stress variations are the result of deglaciation superimposed on a regional stress field dominated by ridge push. However, we suggest that this reduction in horizontal stresses towards the coast in the northern North Sea may be related to rheological changes of sediments during deeper burial because if it is only due to the regional ice loading and unloading, then its effect should also be observed at shallow depth. This is not the case; the reduction in horizontal stress is only observed at depths greater than 1.5 km.

Results from an anisotropy study of the Upper Jurassic organic-rich shales of Hekkingen Formation in the Barents Sea (borehole 7125/1-1) and Draupne Formation in the North Sea (borehole 16/8-3S) (Zadeh et al., 2017) show the moderately high intensity of stress-induced fractures in the Hekkingen Formation compared to the Draupne Formation. Mineralogically, both organic-rich shale formations are rich in kaolinite and contain smectite and illite. Both formations have been exposed to temperatures > 80 °C in the past and are chemically compacted probably related to the smectite to illite and quartz reaction through illite-smectite mixed layer minerals that might have increased the brittleness of the shales in both boreholes (Zadeh et al., 2017). The Draupne shales in borehole 16/8-3S are nearly at their maximum burial depth (<100 m uplift) but the Hekkingen shales in borehole 7125/1-1 are significantly uplifted (~1300 m) (Baig et al., 2016). Therefore, reduced confining pressure by unloading may have caused the higher intensity of stress-induced fractures found in the Barents Sea Hekkingen shales in borehole 7125/1-1 compared to the North Sea Draupne shales in borehole 16/8-3S. Kalani et al. (2015) also observed that microfractures intensity was high in more compacted Upper Jurassic shales in the Egersund Basin.

5.6. Implications for burial and thermal histories

1-D modelling was performed to assess burial and thermal histories in one of the borehole section (17/3-1) located at the boundary between the Ling Depression and Stord Basin (Fig. 2). A minor gas discovery was made in the upper 2 m sands of the Middle Jurassic Sandnes Formation in borehole 17/3-1 (Norwegian Petroleum Directorate, 2013). The 1-D burial and thermal history model was calibrated with the measured vitrinite reflectance and present-day borehole temperature data by using exhumation estimates from the current study (Fig. 16). The reservoir rocks of Sandnes Formation were deposited during the Middle Jurassic, and the source rocks of Tau Formation were deposited during the Late Jurassic in this area. Both the Sandnes and Tau formations have experienced nearly identical burial and temperature histories throughout the basin development in this area and reached to their maximum burial depth of about 2550 to 2650 mbsf during the late Neogene. The area was later uplifted, and more than about 670 m sediments were eroded below the angular unconformity before buried again below ~ 100 m thick sediments of mid-late Quaternary in this area (Fig. 17).

Measured data reflect that pore pressure gradually increases from the Top Upper Jurassic and reaches to 28.37 MPa at the base of the Tau Formation. The pore pressure remains within the range of 24.5 MPa below the Tau Formation (Norwegian Petroleum Directorate, 2013). Petromod 1-D simulation shows minor overpressure in all units below the base of the Shetland Group. The overpressure builds up gradually downward, and maximum pore pressure (28.7 MPa) was detected at the base of the Tau Formation (Fig. 18). The measured data show pore pressure reversal due to most likely lateral connectivity of the sediments below the Tau Formation, but the 1D model considered that there is no lateral connectivity and all units are impermeable and hence failed to capture the regression. Minor overpressure

(<5 MPa) witnessed today within the Tau Formation was established during the late Pliocene-early Pleistocene due to rapid burial and high sedimentation rates of ~300 to 550 m/Ma, but equilibrium is still not reached even after the erosion of these sediments (Fig. 18).

The temperature reached to ~70 °C within the Tau Formation during the Early Cretaceous but remained constant between 65 °C and 70 °C during the next 30 Myr until the Early Paleocene. A gradual temperature increase followed during the Paleocene-Early Eocene after which rapid sedimentation initiated an increase of about 20-30 °C during the Late Eocene-Early Miocene resulting in temperatures close to 100 °C. Temperatures then remained more or less constant during the mid-Miocene hiatus before it decreased to 95 °C during Late Miocene-Pliocene. A second rapid heating phase initiated during late Pliocene-Pleistocene and the maximum temperature values reached to ~105 °C. This was followed by a rapid cooling phase until the present-day values of about 80 °C were reached (Fig. 19).

Vitrinite reflectance values within the Tau Formation remained below 0.53% during the first 120 Myr of the simulated basin development, mainly due to slow sedimentation rates and the high thermal conductivities of the predominantly carbonate lithologies. Vitrinite reflectance values reached the present value of 0.65% during the rapid heating phase in the late Pliocene-early Pleistocene (Fig. 19). The Tau Formation consists of organic matter of kerogen type II and type III, and mineralogically consists of smectite, illite/smectite mixed layers and kaolinitic clays in borehole samples from the Egersund Basin (Kalani et al., 2014, 2015). Observed and modelled vitrinite reflectance data indicate that the Tau Formation is marginally mature (%R <0.65%) and may not have generated large quantities of hydrocarbons in this area. Although the source rock at well location is only marginally mature, it could be more mature in the deeper part of the basin to the southwest and therefore may explain a minor gas discovery in the Sandnes Formation. The modelling indicates that the Tau Formation was exposed to a paleotemperature of about 90 °C to 100 °C during the

Oligocene-Pliocene and reached a maximum paleotemperature of about 105 °C for a very short period of time during the early Pleistocene (Fig. 19). This indicates that the Tau Formation has spent sufficient time at temperatures (70-100 °C) suitable for the transformation of smectite to illite and quartz cementation in shales (Bjørlykke, 1998). The smectite to illite transformation may have changed the rheology of the seal and source rocks from more ductile to more brittle (Dewhurst and Siggins, 2006). Moreover, the brittleness of shales may have resulted in possible fracturing due to unloading during the Quaternary and this fracturing of seal rocks can have significant effects on CO_2 storage and/or the leakage of the hydrocarbons in this area which is also evident by pockmarks observed in several places along the Norwegian Channel (Hovland and Judd, 1988).

6. Conclusions

Well logs and vitrinite reflectance data from a large number of boreholes in the Norwegian and Danish North Sea sectors were analysed in this study. Exhumation is estimated from compaction and thermal maturity techniques. Exhumation estimates are important to predict the rheological properties of the reservoir and seal rocks and modelling the source rock maturity and evolution of overpressure in the exhumed basins. Main findings from this study are summarized below:

- The Central Graben and south Viking Graben areas are currently at their maximum burial depth, whereas no or minor (<100 m) exhumation is estimated on the flanking highs. Basin margin areas are largely affected by the late Neogene exhumation episode, and exhumation estimates are increasing towards east-northeast in the eastern parts and mainly towards east elsewhere in the study area.
- Average exhumation estimates range from ~ 400 to 800 m in the Danish sector, from ~ 100 to 500 m in the central part and <100 to 300 m in the northwestern part in the

Norwegian sector. Average exhumation estimates are ≥ 900 m within the Sorgenfrei-Tornquist Zone area. Average exhumation in the Egersund Basin area range from ~200 m in the west to > 600 m in the east. Average exhumation within the Lista Fault Blocks area varies from ~500 m in the south to >700 m in the north. Average exhumation estimates within the Stord Basin are ~100 to 700 m in the southern part and ~200 to 900 m in the northern part.

- Erosion of sediments may have provoked an isostatic response in the area and surface elevations reduced due to the erosion of the sediments may have been restored 60–70% by the isostatic rebound. Restored surface elevations indicate large subaerially exposed areas before the onset of uplift and erosion in the Norwegian-Danish Basin and along the southwest coast of Norway. This is also supported by predominantly coastal and/or deltaic environments in the Norwegian-Danish Basin area during the late Neogene.
- Early Quaternary to pre-Quaternary strata is truncated below the mid-late Quaternary unconformity indicating that a large amount of sediments are removed below this younger unconformity in the basin margin areas along the southwest coast of Norway. The similarity of exhumation estimates from Early Cretaceous -Early Miocene shales indicates that maximum burial may have taken place later than Early Miocene in most of the areas. Seismic stratigraphic analyses indicate that the maximum burial may have been reached sometime during the Oligocene in the Sorgenfrei-Tornquist Zone area and during the Pliocene in the eastern part of the Norwegian-Danish Basin, whereas sediments reached to their maximum burial during early Quaternary in the western part of the Norwegian-Danish Basin. Sediments are currently at their maximum burial in the Central Graben area.

- Exhumation has diverse effects on rock properties and source rock maturity. The onset of quartz cementation/chemical compaction is observed at depth around 2 km, and present-day temperature at this depth is more than 70 °C in areas of maximum burial depth (e.g. in the Central Graben and south Viking Graben area). The onset of quartz cementation is observed at shallower present-day depths (<1.4 km) due to exhumation in the basin margin areas. The rheology of shales may change from ductile to brittle when shales are cemented, and the ratio between horizontal and vertical effective stresses is reduced. Cemented shales can fracture more easily during unloading under low strain levels, leading to hydrocarbon leakage or seal failure (in case of CO_2 injection).
- 1-D burial and thermal history modelling results suggest that Upper Jurassic source rocks of Tau Formation are early hydrocarbon mature in the Ling Depression area. Maximum paleotemperature was reached during the late Pliocene-early Pleistocene. Modelling results also suggest that the minor overpressure observed today was established due to the rapid burial of the sediments during the late Pliocene-early Pleistocene.

Acknowledgements

We are thankful to Det Norske for funding of the project work through the Centre for Earth Evolution and Dynamics (CEED) projects. Many thanks also go to First Geo for providing us the depth-converted 2D seismic data. We are also thankful to Schlumberger for access to Petrel and PetroMod software at the University of Oslo.

References

Allen, P.A., Allen, J.R., 2013. Basin analysis: Principles and application to petroleum play assessment. John Wiley & Sons.

Anell, I., Thybo, H., Artemieva, I.M., 2009. Cenozoic uplift and subsidence in the North Atlantic region: Geological evidence revisited. Tectonophysics 474, 78-105.

Anell, I., Thybo, H., Rasmussen, E., 2012. A synthesis of Cenozoic sedimentation in the North Sea. Basin Research 24, 154-179.

Angeli, M., Faleide, J.I., Gabrielsen, R.H., 2013. Evaluating Seal Quality for Potential Storage Sites in the Norwegian North Sea. Energy Procedia 37, 4853-4862.

Archard, G., Stafford, J., Bardwell, K., Bagge, M., 1998. A review of techniques used to determine geological and thermal history in the Southern North Sea, pp. 117-136.

Armour, A., Graham, C., Bathurst, P., Evans, D., 2003. The Millennium Atlas: Petroleum Geology of the Central and Northern North Sea. Geological Society of London.

Athy, L.F., 1930. Density, porosity, and compaction of sedimentary rocks. AAPG Bulletin 14, 1-24.

Avseth, P., Mukerji, T., Mavko, G., 2005. Quantitative seismic interpretation: Applying rock physics tools to reduce interpretation risk. Cambridge University Press.

Baig, I., 2018. Burial and thermal histories of sediments in the southwestern Barents Sea and North Sea areas: Evidence from integrated compaction, thermal maturity and seismic stratigraphic analyses, Department of Geosciences. University of Oslo, pp. 1-194.

Baig, I., Faleide, J.I., Jahren, J., Mondol, N.H., 2016. Cenozoic exhumation on the southwestern Barents Shelf: Estimates and uncertainties constrained from compaction and thermal maturity analyses. Marine and Petroleum Geology 73, 105-130.

Barker, C.E., 1989. Temperature and time in the thermal maturation of sedimentary organic matter. Thermal history of basins: methods and case histories: Berlin, Springer-Verlag, 74-98.

Barker, C.E., Pawlewicz, M.J., 1994. Calculation of Vitrinite Reflectance from Thermal Histories and Peak Temperatures, Vitrinite Reflectance as a Maturity Parameter. American Chemical Society, pp. 216-229.

Berre, T., Tunbridge, L., Hoeg, K., 1995. The measurement of small strains and Ko-values in triaxial tests on clay-shales, 8th ISRM Congress. International Society for Rock Mechanics.

Bjørlykke, K., 1998. Clay mineral diagenesis in sedimentary basins; a key to the prediction of rock properties; examples from the North Sea Basin. Clay Minerals 33, 15-34.

Bjørlykke, K., 1999. Principal aspects of compaction and fluid flow in mudstones. Geological Society, London, Special Publications 158, 73-78.

Bjørlykke, K., 2010. Petroleum Geoscience: From Sedimentary Environments to Rock Physics.

Bjørlykke, K., 2014. Relationships between depositional environments, burial history and rock properties. Some principal aspects of diagenetic process in sedimentary basins. Sedimentary Geology 301, 1-14.

Bjørlykke, K., Høeg, K., 1997. Effects of burial diagenesis on stresses, compaction and fluid flow in sedimentary basins. Marine and Petroleum Geology 14, 267-276.

Brekke, H., 2000. The tectonic evolution of the Norwegian Sea continental margin, with emphasis on the Vøring and Møre basins. Special Publication-Geological Society of London 167, 327-378.

Bulat, J., Stoker, S., 1987. Uplift determination from interval velocity studies, UK southern North Sea. Petroleum geology of north-west Europe: London, Graham and Trotman, 293–305.

Burnham, A.K., Sweeney, J.J., 1989. A chemical kinetic model of vitrinite maturation and reflectance. Geochimica et Cosmochimica Acta 53, 2649-2657.

Caillet, G., Judge, N., Bramwell, N., Meciani, L., Green, M., Adam, P., 1997. Overpressure and hydrocarbon trapping in the Chalk of the Norwegian Central Graben. Petroleum Geoscience 3, 33-42.

Cameron, T.D.J., Stoker, M.S., Long, D., 1987. The history of Quaternary sedimentation in the UK sector of the North Sea Basin. Journal - Geological Society (London) 144, 43-58.
Cohen, K., Finney, S., Gibbard, P., Fan, J.-X., 2013. The ICS international chronostratigraphic chart. Episodes 36, 199-204.
Cope, M.J., 1986. An Interpretation of Vitrinite Reflectance Data From the Southern North Sea Basin, Geological Society Special Publication, pp. 85-98.
Corcoran, D., Clayton, G., 1999. Interpretation of vitrinite reflectance profiles in the Central Irish Sea area: Implications for the timing of organic maturation. Journal of Petroleum Geology 22, 261-286.
Corcoran, D.V., Doré, A.G., 2005. A review of techniques for the estimation of magnitude and timing of exhumation in offshore basins. Earth-Science Reviews 72, 129-168.
Dahlgren, K.T., Vorren, T.O., Laberg, J.S., 2002. Late Quaternary glacial development of the mid-Norwegian margin—65 to 68 N. Marine and Petroleum Geology 19, 1089-1113.
Dalland, A., Worsley, D., Ofstad, K., 1988. A Lithostratigraphic Scheme for the Mesozoic and Cenozoic and Succession Offshore Mid-and Northern Norway. Oljedirektoratet.
Dewhurst, D.N., Jones, R.M., 2002. Geomechanical, microstructural, and petrophysical evolution in experimentally reactivated cataclasites: Applications to fault seal prediction. AAPG bulletin 86.
Dewhurst, D.N., Siggins, A.F., 2006. Impact of fabric, microcracks and stress field on shale anisotropy. Geophysical Journal International 165, 135-148.
Doré, A.G., Cartwright, J.A., Stoker, M.S., Turner, J.P., White, N.J., 2002. Exhumation of the North Atlantic margin: Introduction and background, pp. 1-12.
Doré, A.G., Jensen, L.N., 1996. The impact of late Cenozoic uplift and erosion on hydrocarbon exploration: offshore Norway and some other uplifted basins. Global and Planetary Change 12, 415-436.
Dow, W.G., 1977. Kerogen studies and geological interpretations. Journal of geochemical exploration 7, 79-99.
Dörr, N., Lisker, F., Clift, P.D., Carter, A., Gee, D.G., Tebenkov, A.M., Spiegel, C., 2012. Late Mesozoic-Cenozoic exhumation history of northern Svalbard and its regional significance: Constraints from apatite fission track analysis. Tectonophysics 514-517, 81-92.
Edward, K.J., 2011. The Post Triassic uplift and erosion history of the Southwestern UK, School of Geography, Earth & Environmental Sciences. University of Birmingham.
Eidvin, T., Goll, R.M., Grogan, P., Smelror, M., Ulleberg, K., 1998. The Pleistocene to Middle Eocene stratigraphy and geological evolution of the western Barents Sea continental margin at well site 7316/5-1 (Bjørnoya West area). Norsk Geologisk Tidsskrift 78, 99-123.
Eidvin, T., Jansen, E., Riis, F., 1993. Chronology of Tertiary fan deposits off the western Barents Sea: implications for the uplift and erosion history of the Barents Shelf. Marine Geology 112, 109-131.
Eidvin, T., Jansen, E., Rundberg, Y., Brekke, H., Grogan, P., 2000. The upper Cainozoic of the Norwegian continental shelf correlated with the deep sea record of the Norwegian Sea and the North Atlantic. Marine and Petroleum Geology 17, 579-600.
Eidvin, T., Riis, F., 2013. Investigation of Oligocene to Lower Pliocene deposits in the Norwegian shelf: Paleo-geography and development of saline aquifer systems.
Eidvin, T., Riis, F., Rasmussen, E.S., 2014. Oligocene to Lower Pliocene deposits of the Norwegian continental shelf, Norwegian Sea, Svalbard, Denmark and their relation to the uplift of Fennoscandia: A synthesis. Marine and Petroleum Geology 56, 184-221.
Eidvin, T., Rundberg, Y., 2001. Late Cainozoic stratigraphy of the Tampen area (Snorre and Visund fields) in the northern North Sea, with emphasis on the chronology of early Neogene sands. Norsk Geologisk Tidsskrift 81, 119-160.

Faleide, J.I., Bjørlykke, K., Gabrielsen, R.H., 2010. Geology of the Norwegian Continental Shelf. Petroleum Geoscience, 467-499.

Faleide, J.I., Kyrkjebø, R., Kjennerud, T., Gabrielsen, R.H., Jordt, H., Fanavoll, S., Bjerke, M.D., 2002. Tectonic impact on sedimentary processes during Cenozoic evolution of the northern North Sea and surrounding areas. Geological Society, London, Special Publications 196, 235-269.

Fawad, M., Mondol, N.H., Jahren, J., Bjørlykke, K., 2010. Microfabric and rock properties of experimentally compressed silt-clay mixtures. Marine and Petroleum Geology 27, 1698-1712.

Gabrielsen, R.H., Færseth, R.B., Steel, R.J., Idil, S., Klovjan, O.S., 1990. Architectural styles of basin fill in the northern Viking Graben, Tectonic evolution of the North Sea rifts, pp. 158-179.

Ghazi, S.A., 1992. Cenozoic uplift in the Stord Basin area and its consequences for exploration. Norsk Geologisk Tidsskrift 72, 285-290.

Gilchrist, A., Summerfield, M., Cockburn, H., 1994. Landscape dissection, isostatic uplift, and the morphologic development of orogens. Geology 22, 963-966.

Green, P.F., Duddy, I.R., Japsen, P., 2017. Multiple episodes of regional exhumation and inversion identified in the UK Southern North Sea based on integration of palaeothermal and palaeoburial indicators, Geological Society, London, Petroleum Geology Conference series. Geological Society of London, p. PGC8. 21.

Grollimund, B., Zoback, M.D., 2000. Post glacial lithospheric flexure and induced stresses and pore pressure changes in the northern North Sea. Tectonophysics 327, 61-81.

Hacquebard, P., Donaldson, J., 1970. Coal metamorphism and hydrocarbon potential in the Upper Paleozoic of the Atlantic Provinces, Canada. Canadian Journal of Earth Sciences 7, 1139-1163.

Hansen, S., 1996. Quantification of net uplift and erosion on the Norwegian Shelf south of 66° N from sonic transit times of shale. Norsk Geologisk Tidsskrift 76, 245-252.

Heasler, H.P., Kharitonova, N.A., 1996. Analysis of sonic well logs applied to erosion estimates in the Bighorn basin, Wyoming. AAPG Bulletin 80, 630-646.

Henriksen, E., Bjørnseth, H., Hals, T., Heide, T., Kiryukhina, T., Kløvjan, O., Larssen, G., Ryseth, A., Rønning, K., Sollid, K., 2011. Uplift and erosion of the greater Barents Sea: impact on prospectivity and petroleum systems. Geological Society, London, Memoirs 35, 271-281.

Hillis, R.R., 1995. Quantification of Tertiary exhumation in the United Kingdom southern North Sea using sonic velocity data. Aapg Bulletin-American Association of Petroleum Geologists 79, 130-152.

Hoshino, K., Koide, H., Inami, K., lwamura, S., Mitsui, S., 1972. Mechanical properties of Japanese Tertiary sedimentary rocks under high confining pressures, Geol. Surv. Japan Rep, pp. 1-229.

Hovland, M., Judd, A., 1988. Seabed pockmarks and seepages: impact on geology, biology, and the marine environment. Springer.

Huuse, M., 2002. Cenozoic uplift and denudation of southern Norway: Insights from the North Sea Basin, pp. 209-233.

Isaksen, D., Tonstad, K., 1989. A revised Cretaceous and Tertiary lithostratigraphic nomenclature for the Norwegian North Sea. Norwegian Petroleum Directorate.

Jansen, E., Sjøholm, J., 1991. Reconstruction of glaciation over the past 6 Myr from ice-borne deposits in the Norwegian Sea. Nature 349, 600-603.

Japsen, P., 1993. Influence of lithology and Neogene uplift on seismic velocities in Denmark: implications for depth conversion of maps. American Association of Petroleum Geologists Bulletin 77, 194-211.

Japsen, P., 1998. Regional velocity-depth anomalies, North Sea Chalk: A record of overpressure and Neogene uplift and erosion. AAPG Bulletin 82, 2031-2074.

Japsen, P., 1999. Overpressured Cenozoic shale mapped from velocity anomalies relative to a baseline for marine shale, North Sea. Petroleum Geoscience 5, 321-336.

Japsen, P., 2000. Investigation of multi-phase erosion using reconstructed shale trends based on sonic data. Sole Pit axis, North Sea. Global and Planetary Change 24, 189-210.

Japsen, P., 2017. Sonic velocity of chalk, sandstone and marine shale controlled by effective stress: Velocity-depth anomalies as a proxy for vertical movements. Gondwana Research.

Japsen, P., Bidstrup, T., 1999. Quantification of late Cenozoic erosion in Denmark based on sonic data and basin modelling. Bulletin of the Geological Society of Denmark 46, 79-99.

Japsen, P., Bidstrup, T., Lidmar-Bergstrom, K., 2002. Neogene uplift and erosion of southern Scandinavia induced by the rise of the South Swedish Dome. Special publication-Geological Society Of London 196, 183-208.

Japsen, P., Chalmers, J.A., 2000. Neogene uplift and tectonics around the North Atlantic: Overview. Global and Planetary Change 24, 165-173.

Japsen, P., Green, P.F., Bonow, J.M., Rasmussen, E.S., Chalmers, J.A., Kjennerud, T., 2010. Episodic uplift and exhumation along North Atlantic passive margins: implications for hydrocarbon prospectivity. Geological Society, London, Petroleum Geology Conference series 7, 979-1004.

Japsen, P., Green, P.F., Nielsen, L.H., Rasmussen, E.S., Bidstrup, T., 2007. Mesozoic-Cenozoic exhumation events in the eastern North Sea Basin: a multi-disciplinary study based on palaeothermal, palaeoburial, stratigraphic and seismic data. Basin Research 19, 451-490.

Japsen, P., Rasmussen, E.S., Green, P.F., Nielsen, L.H., Bidstrup, T., 2008. Cenozoic palaeogeography and isochores predating the Neogene exhumation of the eastern North Sea Basin, pp. 25-28.

Jarsve, E.M., Eidvin, T., Nystuen, J.P., Faleide, J.I., Gabrielsen, R.H., Thyberg, B.I., 2014a. The Oligocene succession in the Eastern North Sea: Basin development and depositional systems. Geological Magazine 108.

Jarsve, E.M., Faleide, J.I., Gabrielsen, R.H., Nystuen, J.P., 2014b. Mesozoic and Cenozoic basin configurations in the North Sea, From Depositional Systems to Sedimentary Successions on the Norwegian Continental Margin. John Wiley & Sons, Ltd, pp. 417-452.

Jensen, L., Schmidt, B., 1993. Neogene uplift and erosion offshore south Norway; magnitude and consequences for hydrocarbon exploration in the Farsund Basin. Generation, accumulation, and production of Europe’s hydrocarbons, III: Berlin, Springer Verlag, 79–88.

Jensen, L.N., Schmidt, B.J., 1992. Late Tertiary uplift and erosion in the Skagerrak area: magnitude and consequences. Norsk Geologisk Tidsskrift 72, 275-279.

Jordt, H., Thyberg, B.I., Nøttvedt, A., 2000. Cenozoic evolution of the central and northern North Sea with focus on differential vertical movements of the basin floor and surrounding clastic source areas, Geological Society Special Publication, pp. 219-243.

Kalani, M., Jahren, J., Mondol, N.H., Faleide, J.I., 2014. Compaction processes and rock properties in uplifted clay dominated units– the Egersund Basin, Norwegian North Sea. Marine and Petroleum Geology 68, 596-613.

Kalani, M., Jahren, J., Mondol, N.H., Faleide, J.I., 2015. Petrophysical implications of source rock microfracturing. International Journal of Coal Geology 143, 43-67.

King, C., 2016. A revised correlation of Tertiary rocks in the British Isles and adjacent areas of NW Europe.

Kleiven, H.F., Jansen, E., Fronval, T., Smith, T., 2002. Intensification of Northern Hemisphere glaciations in the circum Atlantic region (3.5–2.4 Ma)–ice-rafted detritus evidence. Palaeogeography, Palaeoclimatology, Palaeoecology 184, 213-223.

Kyrkjebø, R., Hamborg, M., Faleide, J.I., Jordt, H., Christiansson, P., 2000. Cenozoic tectonic subsidence from 2D depositional simulations of a regional transect in the northern North Sea basin, Geological Society Special Publication, pp. 273-294.

Lee, J.R., Busschers, F.S., Sejrup, H.P., 2012. Pre-Weichselian Quaternary glaciations of the British Isles, The Netherlands, Norway and adjacent marine areas south of 68°N: Implications for long-term ice sheet development in northern Europe. Quaternary Science Reviews 44, 213-228.

Lerche, I., Yarzab, R.F., Kendall, C.G.S.C., 1984. Determination of paleoheat flux from vitrinite reflectance data. American Association of Petroleum Geologists Bulletin 68, 1704-1717.

Løseth, H., Henriksen, S., 2005. A Middle to Late Miocene compression phase along the Norwegian passive margin, Geological Society, London, Petroleum Geology Conference series. Geological Society of London, pp. 845-859.

Magara, K., 1976. Thickness of removed sedimentary rocks, paleopore pressure, and paleotemperature, southwestern part of Western Canada Basin. AAPG Bulletin 60, 554.

Mangerud, J., Gyllencreutz, R., Lohne, Ø., Svendsen, J.I., 2011. Chapter 22 - Glacial History of Norway, in: Jürgen Ehlers, P.L.G., Philip, D.H. (Eds.), Developments in Quaternary Sciences. Elsevier, pp. 279-298.

Marcussen, Ø., 2009. Compaction of siliceous sediments : Implications for basin modeling and seismic interpretation. University of Oslo.

Marion, D., Nur, A., Yin, H., Han, D.-H., 1992. Compressional velocity and porosity in sand-clay mixtures. Geophysics 57, 554-563.

Mavromatidis, A., 2006. Burial/exhumation histories for the Cooper–Eromanga Basins and implications for hydrocarbon exploration, Eastern Australia. Basin Research 18, 351-373.

Mavromatidis, A., Hillis, R., 2005. Quantification of exhumation in the Eromanga Basin and its implications for hydrocarbon exploration. Petroleum Geoscience 11, 79-92.

Menpes, R.J., Hillis, R.R., 1995. Quantification of Tertiary exhumation from sonic velocity data, Celtic Sea/South-Western Approaches. Geological Society, London, Special Publications 88, 191-207.

Middleton, M.F., 1982. Tectonic history from vitrinite reflectance. Geophysical Journal of the Royal Astronomical Society 68, 121-132.

Mondol, N.H., Bjørlykke, K., Jahren, J., Høeg, K., 2007. Experimental mechanical compaction of clay mineral aggregates-Changes in physical properties of mudstones during burial. Marine and Petroleum Geology 24, 289-311.

Mukhopadhyay, P., 1992. Maturation of organic matter as revealed by microscopic methods: applications and limitations of vitrinite reflectance, and continuous spectral and pulsed laser fluorescence spectroscopy. Developments in Sedimentology 47, 435-510.

Mukhopadhyay, P.K., Dow, W.G., 1994. Vitrinite reflectance as a maturity parameter.

Nielsen, L.H., Japsen, P., 1991. Deep wells in Denmark 1935-1990: lithostratigraphic subdivision. Danmarks Geologiske Undersogelse, Serie A 31.

Nielsen, S., Clausen, O., McGregor, E., 2017. Basin% Ro: a vitrinite reflectance model derived from basin and laboratory data. Basin Research 29, 515-536.

Nielsen, T., Mathiesen, A., Bryde-Auken, M., 2008. Base Quaternary in the Danish parts of the North Sea and Skagerrak. Geological Survey of Denmark and Greenland Bulletin 15, 37-40.

Norwegian Petroleum Directorate, 2013. The Norwegian Petroleum Directorate Fact-pages of exploration wellbores.

Norwegian Petroleum Directorate, 2018. The Norwegian Petroleum Directorate Fact-pages.

Nygård, A., Sejrup, H.P., Haflidason, H., Bryn, P., 2005. The glacial North Sea Fan, southern Norwegian Margin: Architecture and evolution from the upper continental slope to the deep-sea basin. Marine and Petroleum Geology 22, 71-84.

Nygård, A., Sejrup, H.P., Haflidason, H., Lekens, W.A.H., Clark, C.D., Bigg, G.R., 2007. Extreme sediment and ice discharge from marine-based ice streams: New evidence from the North Sea. Geology 35, 395-398.

Nygård, R., Gutierrez, M., Gautam, R., Høeg, K., 2004. Compaction behavior of argillaceous sediments as function of diagenesis. Marine and Petroleum Geology 21, 349-362.

Rasmussen, E.S., 2004. Stratigraphy and depositional evolution of the uppermost Oligocene–Miocene succession in western Denmark. Bulletin of the Geological Society of Denmark 51, 89-109.

Rasmussen, E.S., VejbæK, O.V., Bidstrup, T., Piasecki, S., DybkjæR, K., 2005. Late Cenozoic depositional history of the Danish North Sea Basin: Implications for the petroleum systems in the Kraka, Halfdan, Siri and Nini fields, Petroleum Geology Conference Proceedings, pp. 1347-1358.

Riis, F., 1996. Quantification of Cenozoic vertical movements of Scandinavia by correlation of morphological surfaces with offshore data. Global and Planetary Change 12, 331-357.

Rohrman, M., Beek, P., Andriessen, P., Cloetingh, S., 1995. Meso - Cenozoic morphotectonic evolution of southern Norway: Neogene domal uplift inferred from apatite fission track thermochronology. Tectonics 14, 704-718.

Rundberg, Y., Eidvin, T., 2005. Controls on depositional history and architecture of the Oligocene-Miocene succession, northern North Sea Basin, Norwegian Petroleum Society Special Publications, pp. 207-239.

Sales, J.K., 1993. Closure vs. seal capacity—A fundamental control on the distribution of oil and gas. Basin modeling: Advances and application: Norwegian Petroleum Society (NPF) Special Publication 3, 399-414.

Sclater, J.G., Christie, P., 1980. Continental stretching: An explanation of the Post - Mid - Cretaceous subsidence of the central North Sea Basin. Journal of Geophysical Research: Solid Earth (1978–2012) 85, 3711-3739.

Sejrup, H.P., 1995. Quaternary of the Norwegian Channel: glaciation history and palaeoceanography. Norsk Geologisk Tidsskrift 75, 65-87.

Sejrup, H.P., Hjelstuen, B.O., Dahlgren, K.I.T., Haflidason, H., Kuijpers, A., Nygård, A., Praeg, D., Stoker, M.S., Vorren, T.O., 2005. Pleistocene glacial history of the NW European continental margin. Marine and Petroleum Geology 22, 1111-1129.

Sejrup, H.P., King, E.L., Aarseth, I., Haflidason, H., Elverhøi, A., 1996. Quaternary erosion and depositional processes: Western Norwegian fjords, Norwegian Channel and North Sea Fan, Geological Society Special Publication, pp. 187-202.

Sejrup, H.P., Larsen, E., Haflidason, H., Berstad, I.M., Hjelstuen, B.O., Jonsdottir, H.E., King, E.L., Landvik, J., Longva, O., Nygard, A., Ottesen, D., Raunholm, S., Rise, L., Stalsberg, K., 2003. Configuration, history and impact of the Norwegian Channel Ice Stream. Boreas 32, 18-36.

Sejrup, H.P., Larsen, E., Landvik, J., King, E.L., Haflidason, H., Nesje, A., 2000. Quaternary glaciations in southern Fennoscandia: Evidence from southwestern Norway and the northern North Sea region. Quaternary Science Reviews 19, 667-685.

Stoker, M., Leslie, A., Scott, W., Briden, J., Hine, N., Harland, R., Wilkinson, I., Evans, D., Ardus, D., 1994. A record of late Cenozoic stratigraphy, sedimentation and climate change from the Hebrides Slope, NE Atlantic Ocean. Journal of the Geological Society 151, 235-249.

Stoker, M.S., Praeg, D., Hjelstuen, B.O., Laberg, J.S., Nielsen, T., Shannon, P.M., 2005. Neogene stratigraphy and the sedimentary and oceanographic development of the NW European Atlantic margin. Marine and Petroleum Geology 22, 977-1005.

Storvoll, V., Bjørlykke, K., Mondol, N.H., 2005. Velocity-depth trends in Mesozoic and Cenozoic sediments from the Norwegian Shelf. AAPG bulletin 89, 359-381.

Storvoll, V., Brevik, I., 2008. Identifying time, temperature, and mineralogical effects on chemical compaction in shales by rock physics relations. Leading Edge (Tulsa, OK) 27, 750-756.

Suggate, R.P., 1998. Relations between depth of burial, vitrinite reflectance and geothermal gradient. Journal of Petroleum Geology 21, 5-32.

Surlyk, F., Dons, T., Clausen, C., Higham, J., 2003. Upper cretaceous, in: Armour, A., Graham, C., Bathurst, P., Evans, D. (Eds.), The Millennium Atlas: Petroleum Geology of the Central and Northern North Sea. Geological Society of London London.

Sweeney, J.J., Burnham, A.K., 1990. Evaluation of a simple model of vitrinite reflectance based on chemical kinetics. AAPG Bulletin 74, 1559-1570.
Tassone, D.R., Holford, S.P., Duddy, I.R., Green, P.F., Hillis, R.R., 2014. Quantifying Cretaceous–Cenozoic exhumation in the Otway Basin, southeastern Australia, using sonic transit time data: Implications for conventional and unconventional hydrocarbon prospectivity. AAPG Bulletin 98, 67-117.
Thyberg, B., Jahren, J., 2011. Quartz Cementation in Mudstones: Sheet-Like Quartz Cement from Clay Mineral Reactions during Burial. Petroleum Geoscience 17, 53-63.
Thyberg, B., Jahren, J., Winje, T., Bjørlykke, K., Faleide, J.I., Marcussen, Ø., 2010. Quartz cementation in Late Cretaceous mudstones, northern North Sea: Changes in rock properties due to dissolution of smectite and precipitation of micro-quartz crystals. Marine and Petroleum Geology 27, 1752-1764.
Tissot, B., Pelet, R., Ungerer, P., 1987. Thermal history of sedimentary basins, maturation indices, and kinetics of oil and gas generation. AAPG bulletin 71, 1445-1466.
Underdown, R., Redfern, J., Lisker, F., 2007. Constraining the burial history of the Ghadames Basin, North Africa: an integrated analysis using sonic velocities, vitrinite reflectance data and apatite fission track ages. Basin Research 19, 557-578.
Waples, D.W., 1980a. Time and temperature in petroleum formation: application of Lopatin's method to petroleum exploration. AAPG bulletin 64, 916-926.
Waples, D.W., 1980b. Time and temperature in petroleum formation: application of Lopatin's method to petroleum exploration. American Association of Petroleum Geologists Bulletin 64, 916-926.
Waples, D.W., 1984. Thermal models for oil generation.
Waples, D.W., 1994a. Maturity Modeling: Thermal Indicators, Hydrocarbon Generation, and Oil Cracking: Chapter 17: Part IV. Identification and Characterization.
Waples, D.W., 1994b. Modeling of sedimentary basins and petroleum systems. The petroleum system - from source to trap, 307-322.
Watts, A.B., 2001. Isostasy and Flexure of the Lithosphere. Cambridge University Press.
Zadeh, M.K., Mondol, N.H., Jahren, J., 2017. Velocity anisotropy of Upper Jurassic organic-rich shales, Norwegian Continental Shelf. Geophysics 82, C61-C75.
Ziegler, P.A., 1975. North Sea basin history in the tectonic framework of north-western Europe. Geol 1, 131-149.
Ziegler, P.A., 1978. North-western Europe: Tectonics and basin development. Geologie en Mijnbouw 57, 589-626.
Ziegler, P.A., 1990a. Collision related intra-plate compression deformations in Western and Central Europe. Journal of Geodynamics 11, 357-388.
Ziegler, P.A., 1990b. Tectonic and palaeogeographic development of the North Sea rift system. Tectonic evolution of the North Sea rifts, 1-36.

Figures Captions

Fig. 1. Subcrop geology map below the angular unconformity. The column to the right shows simplified Jurassic-Quaternary lithostratigraphy of the study area. Modified after Dalland et al. (1988), Isaksen and Tonstad (1989), Japsen et al. (2007), Bjørlykke (2010) Jarsve et al. (2014b) and Baig (2018).

Fig. 2. Map showing the location of the study area with structural elements and data available during this study. Structural elements map is modified after NPD (2011). Boreholes with data from only well logs are shown with open diamond symbols, boreholes with data from both well logs and vitrinite reflectance are shown with filled diamond, and open triangles indicate additional data samples along depth converted seismic sections. Black lines mark the three transects discussed in the text. Red line marks the approximate eastern boundary of the reference areas. Boreholes to the west of this boundary were used to establish normal compaction trends in this study. The broken blue line marks the boundary of the Norwegian Channel. ESB, Egersund Basin; FSB, Farsund Basin; FT, Fjerritslev Trough; JH, Jæren High; LD, Ling Depression; LFB, Lista Fault Block; MFB, Moray Firth Basin; PBR, Patch Bank Ridge; RFH, Ringkøbing-Fyn High; SB, Stord Basin; SeH, Selle High; SH, Sørvestlandet High; SP, Stavanger Platform; STZ, Sorgenfrei-Tornquist Zone; ÅG, Åsta Graben; ØFC, Øygarden Fault Complex.

Fig. 3. The methodology adopted for this study is based on compaction analyses. (a) Porosity versus shear modulus showing two distinct trends (mechanical and chemical compactions) and velocity variations within each zone. (b) An example of interval transit time versus depth cross-plot to estimate compaction coefficient. (c) Sonic velocity versus depth cross-plot showing normal compaction curves for hydrostatically pressured shales and chalk established in areas currently at their maximum burial. High over-pressure areas are shown in the index

map in Fig. 4. Normal compaction curves 3-8 correspond to equations 3-8 discussed in the text. Normal compaction curves for Cretaceous and Paleogene shales (i, ii) in the southwestern Barents Sea from Baig et al. (2016) and for Danian chalk (iii, iv) in the North Sea from Japsen (2000) and Japsen (2017) are also shown for reference. An example of sonic velocity data from an exhumed well (17/3-1 given in the index map of Fig. 4) is also shown for illustration. Vertical arrows are showing the magnitude of exhumation, and horizontal arrows are showing the velocity variations at the shallow and deeper burial depths.

Fig. 4. Vitrinite reflectance data from exhumed and non-exhumed boreholes are plotted on a semi-logarithmic scale. The predicted thermal maturity curves by assuming a constant heating rate of 1 °C/Ma and geothermal gradient of 30 °C/km, 35 °C/km, and 40 °C/km are also shown for reference from Burnham and Sweeney (1989). Inset map shows the location of exhumed (17/3-1) and non-exhumed (2/7-2) wells together with contours of chalk overpressure (5, 10, 15 MPa) from Japsen (1998). Overpressure is decreasing outwards. Red line marks the approximate boundary between exhumed areas to the east and non-exhumed areas to the west.

Fig. 5. Estimated net exhumation maps from, (a) sonic logs, (b) vitrinite reflectance data, (c) difference in exhumation between estimates from sonic and vitrinite reflectance data, and (d) average exhumation from the two datasets. Source data points used to generate these maps are also shown for reference.

Fig. 6. Maps based on the 1D isostatic adjustment of the area showing, (a) isostatic uplift of the area due to removal of sediments, (b) isostatic subsidence due to loading by water/sediments, (c) total change in the elevation after the uplift/erosion and (d) paleo-surface elevation restored to the onset of uplift and erosion. See text for detail explanation of these maps.

Fig. 7. (a-c) Comparison of exhumation estimates with the published studies along three depth-converted seismic transects.

Fig. 8. Comparison of net exhumation estimates from (Late Cretaceous-Early Paleocene Shetland Group carbonates/shales with the net exhumation estimates from Eocene-Early. Miocene Hordaland Group shales, Paleocene-Eocene Rogaland Group shales and Early. Cretaceous Cromer Knoll Group shales.

Fig. 9. The lower section shows an illustration of Cenozoic seismic stratigraphy along a WSW-ENE oriented composite seismic line. Late Cretaceous to Oligocene strata is truncated below the latest Oligocene horizon towards east-northeast of borehole Inez-1, whereas Miocene to early Quaternary strata is truncated below the mid-late Quaternary unconformity which also has reworked the latest Oligocene unconformity to the east. Broken lines indicate projected seismic stratigraphic surfaces. The upper section shows exhumation magnitudes along this transect. Chronostratigraphic constraints are from Jarsve et al. (2014a) and Baig (2018). RFH, Ringkøbing-Fyn High; STZ, Sorgenfrei-Tornquist Zone.

Fig. 10. Simplified 1-D burial history of sediments at (a) Felicia-1 and (b) Inez-1 well locations. Burial history diagrams are showing the timing of maximum burial depth and different events of uplift and erosion at both well locations. Felicie-1 well was affected by probably two major uplift and erosion events whereas Inez-1 was affected by mainly a single event during the Cenozoic. Both wells are shown in Fig. 9.

Fig. 11. The approximate position of offlap breaks through the early Quaternary sequence CSS-8 are overlayed on the paleo-surface elevation before the onset of erosion. Possible shorelines can be placed to the east of these offlap breaks. Solid blue and green lines indicate the position of offlap breaks at the beginning of Quaternary (~2.6 Ma) and ~1.2 Ma, respectively, whereas the broken lines indicate west and northwest migration of the offlap

breaks between ~2.6 and ~1.2 Ma (Baig, 2018). Broken blue line along the southwest coast of Norway marks the outline of the Norwegian Channel.

Fig. 12. (a-f) Velocity data through Cretaceous to Quaternary shales in the central North Sea. Highlighted areas show the likely range of velocities (2400-2600 m/s) expected at the onset of chemical compaction.

Fig. 13. Comparison of exhumed (17/3-1) and non-exhumed (2/7-2) wells, (a) showing velocity-depth data colour coded with present-day temperature (TempWb) and, (b) with maximum paleotemperature (TempVR) where vitrinite reflectance data are available. See Fig. 2 for well locations.

Fig. 14. (a) Present-day geothermal gradient map created from Horner-corrected bottom hole temperature in the study area, and (b) map of the observed depth of chemical compaction onset in the background is superimposed with black colour contours of the present-day temperature at this transition. Red line marks the boundary between areas currently at their maximum burial depth to the west and exhumed areas to east. The overlay map shows cooler temperature (<60 °C) at the observed depth of onset of chemical compaction to the east due to uplift and erosion of the overburden.

Fig. 15. Minimum horizontal stress gradients established from leak off tests data in (a) the central North Sea, and (b) the northern North Sea. The inset map shows the contours of overpressure (5, 10, 15 MPa) in chalk from Japsen (1998) superimposed on average exhumation map. Overpressure and minimum horizontal stress are decreasing outwards the east.

Fig. 16. Calibration of predicted temperature and vitrinite reflectance with the measured data in borehole 17/3-1.

Fig. 17. Burial history curve superimposed with paleotemperature at 17/3-1 well location.

Fig. 18. Calibration of measured and predicted pore pressure in well 17/3-1.

Fig. 19. Thermal maturity evolution and overpressure built-up during Cenozoic within the Tau Formation in well 17/3-1.

Tables

Table 1. Exhumation estimates from compaction techniques through different lithostratigraphic units and their comparison with exhumation estimates from vitrinite reflectance data. Well locations are given in Fig. 2.

Well	Exhumation from Eocene-Early Miocene shales (m)	Exhumation from Paleocene-Eocene shales (m)	Exhumation from Late Cretaceous-Early Paleocene carbonates/shales (m)	Exhumation from Early Cretaceous Shales (m)	Exhumation from vitrinite reflectance (m)
8/3-2	340	350	290	340	270
8/12-1			80	80	130
9/2-2	550		550	580	480
9/3-1	570		640	670	630
9/8-1	410		490	370	360
9/4-1	330		340	300	280
9/12-1	390	410	460	410	420
10/7-1			670	660	690
11/10-1	550		590	490	590
Inez-1		470	670	510	
Felicia-1			970	920	960
17/3-1			540	590	610
17/4-1	220	170	200	170	210
17/9-1	490	510	510	450	460
17/11-1	260	240	240	250	210
17/12-2	340	280	320	270	320
26/4-1	30		50	30	20
31/4-4	120	120	150	130	70
31/6-3		450	860	730	690
35/1-1	90	70	40	80	
35/11-6	220		340	370	310
36/1-1	640		860		810
36/7-1			860	910	860
6204/11-2		580	530	510	470

Table 2. Comparison of exhumation estimates along transect-3 shown in Fig**.** 2.

Well	**Transect**	**this study**	**Riis (1996)**	**Dore & Jensen (1996)**	**Jensen (1992)**	**Japsen (1998)**
1/5-4	transect-3	0	0	0	0	0
1/6-4	transect-3	0	0	0	0	0
1/3-1	transect-3	0	0	0	0	0
1/3-8	transect-3	0	0	0	0	0
1/3-3	transect-3	0	0	0	0	0
2/1-10	transect-3	0	0	0	0	0
8/10-2	transect-3	0	0	0	0	0
9/4-1	transect-3	300	40	0	0	230
9/4-4	transect-3	390	110	0	140	310
9/2-11	transect-3	560	220	430	440	420

Table 3. Comparison of exhumation estimates along transect-1 shown in Fig. 2.

Well	**Transect**	**this study**	**Riis (1996)**	**Dore & Jensen (1996)**
34/10-8	transect-1	0	0	0
34/11-3	transect-1	30	0	0
31/2-15	transect-1	360	0	0
31/2-6	transect-1	410	30	0
32/2-1	transect-1	970	390	470

Appendix-1

Fig. 20. Lateral and vertical variations in velocities through shales and carbonates along the transect-3 shown in Fig. 2. (a) Average velocity variations along the transect through Hordaland, Rogaland and Cromer Knoll group shales and Shetland group carbonates, (b) vertical variations in velocity through Hordaland Group shales, (c) vertical variations in velocity through Rogaland Group shales, (d) vertical variations in velocity through Shetland Group carbonates and (e) vertical variations in velocity through Cromer Knoll Group shales.

Fig. 21. Lateral and vertical variations in velocities through shales and carbonates along the transect-2 shown in Fig. 2. (a) Average velocity variations along the transect through

Hordaland, Rogaland and Cromer Knoll group shales and Shetland group carbonates, (b) vertical variations in velocity through Hordaland Group shales, (c) vertical variations in velocity through Rogaland Group shales, (d) vertical variations in velocity through Shetland Group shales/carbonates and (e) vertical variations in velocity through Cromer Knoll Group shales.

Fig. 22. Lateral and vertical variations in velocities through shales along the transect-1 shown in Fig. 2. (a) Average velocity variations along the transect through Hordaland, Rogaland, Shetland and Cromer Knoll group shales, (b) vertical variations in velocity through Hordaland Group shales, (c) vertical variations in velocity through Rogaland Group shales, (d) vertical variations in velocity through Shetland Group shales and (e) vertical variations in velocity through Cromer Knoll Group shales.

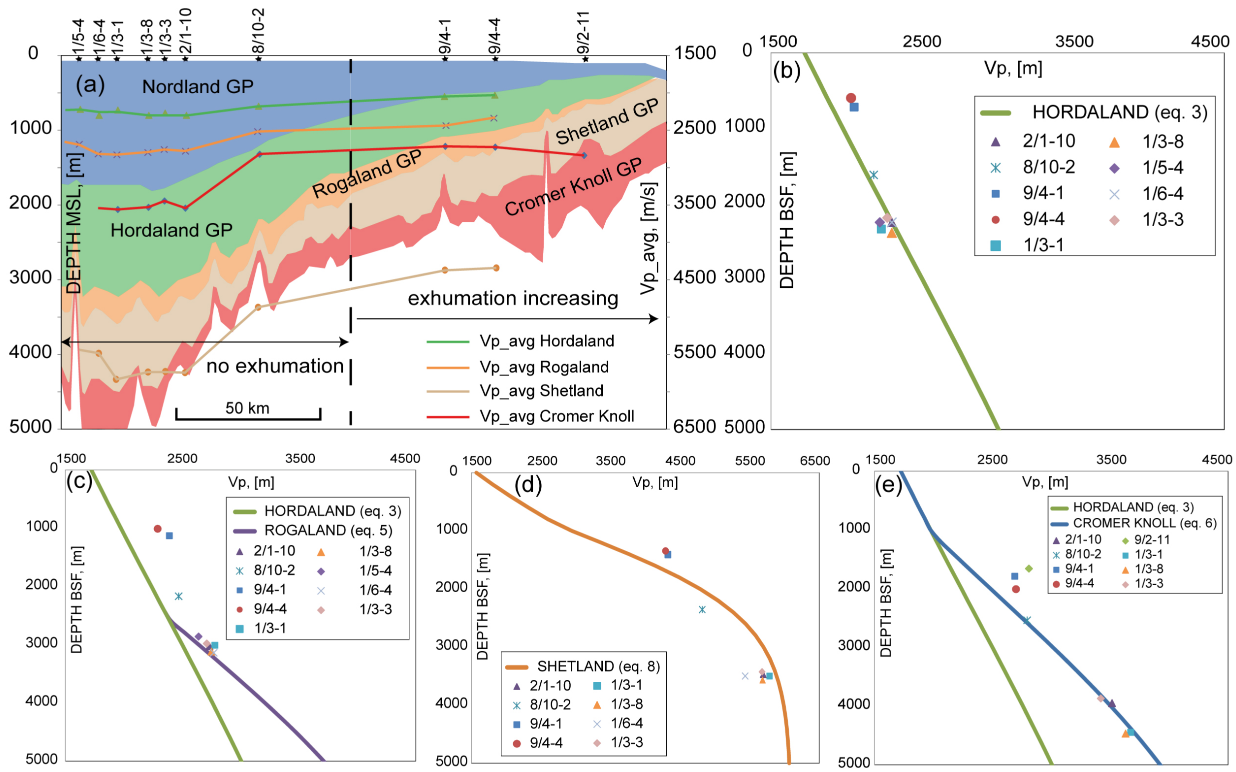

1/5-4
1/6-4
1/3-1
1/3-8
1/3-3
2/1-10
8/10-2
9/4-1
9/4-4
9/2-11
(a)
Nordland GP
Hordaland GP
Rogaland GP
Shetland GP
Cromer Knoll GP
DEPTH MSL, [m]
Vp_avg, [m/s]
exhumation increasing
no exhumation
50 km
Vp_avg Hordaland
Vp_avg Rogaland
Vp_avg Shetland
Vp_avg Cromer Knoll
(b)
Vp, [m]
DEPTH BSF, [m]
HORDALAND (eq. 3)
2/1-10
8/10-2
9/4-1
9/4-4
1/3-1
1/3-8
1/5-4
1/6-4
1/3-3
(c)
ROGALAND (eq. 5)
(d)
SHETLAND (eq. 8)
(e)
CROMER KNOLL (eq. 6)
9/2-11

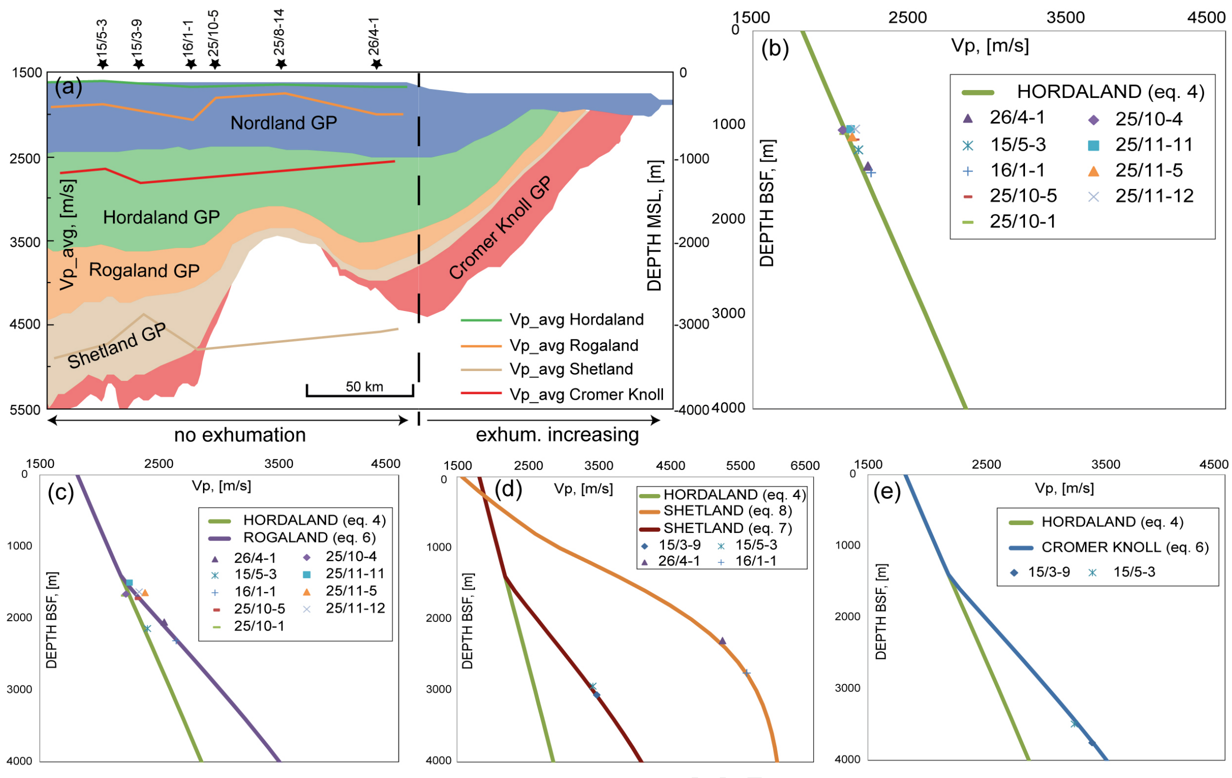

15/5-3
15/3-9
16/1-1
25/10-5
25/8-14
26/4-1
(a)
Nordland GP
Hordaland GP
Rogaland GP
Shetland GP
Cromer Knoll GP
Vp_avg, [m/s]
DEPTH MSL, [m]
Vp_avg Hordaland
Vp_avg Rogaland
Vp_avg Shetland
Vp_avg Cromer Knoll
50 km
no exhumation
exhum. increasing
(b)
Vp, [m/s]
DEPTH BSF, [m]
HORDALAND (eq. 4)
26/4-1
25/10-4
15/5-3
25/11-11
16/1-1
25/11-5
25/10-5
25/11-12
25/10-1
(c)
ROGALAND (eq. 6)
(d)
SHETLAND (eq. 8)
SHETLAND (eq. 7)
15/3-9
(e)
CROMER KNOLL (eq. 6)

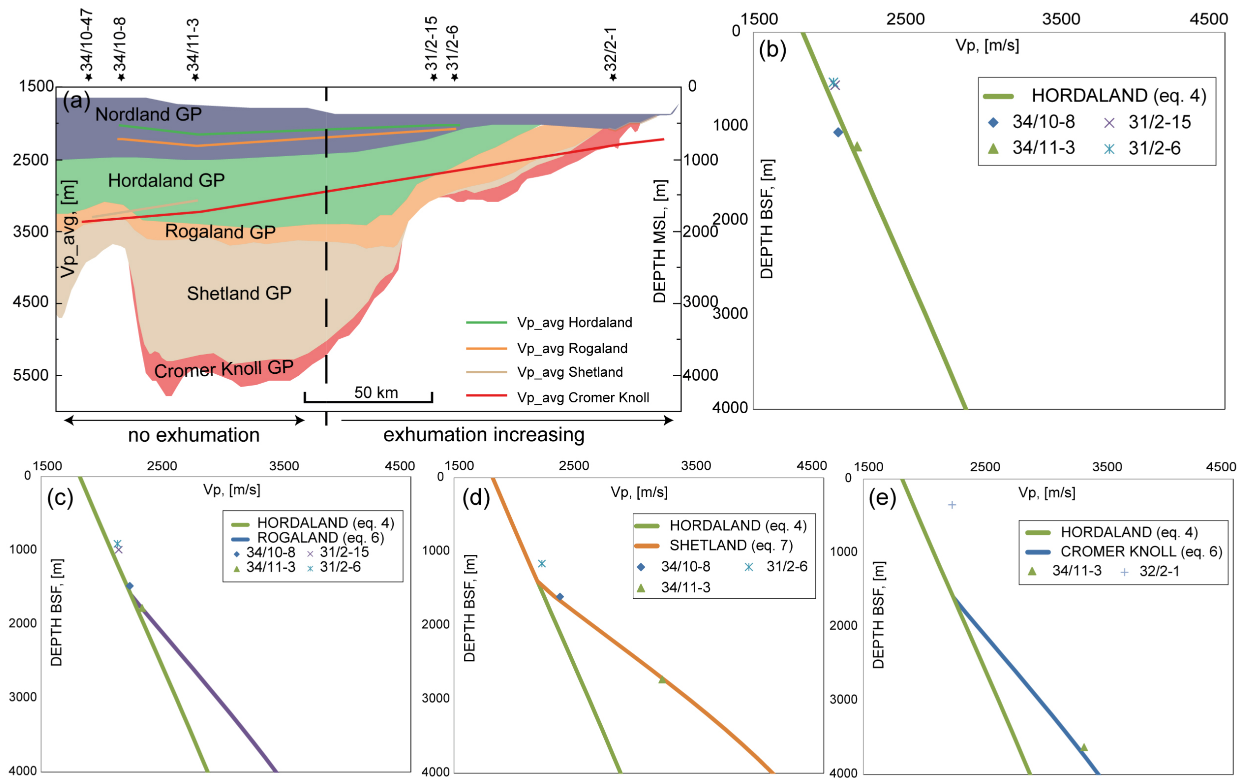
34/10-47
34/10-8
34/11-3
31/2-15
31/2-6
32/2-1
(a)
Nordland GP
Hordaland GP
Rogaland GP
Shetland GP
Cromer Knoll GP
Vp_avg, [m]
DEPTH MSL, [m]
Vp_avg Hordaland
Vp_avg Rogaland
Vp_avg Shetland
Vp_avg Cromer Knoll
50 km
no exhumation
exhumation increasing
(b)
Vp, [m/s]
DEPTH BSF, [m]
HORDALAND (eq. 4)
34/10-8
31/2-15
34/11-3
31/2-6
(c)
HORDALAND (eq. 4)
ROGALAND (eq. 6)
(d)
HORDALAND (eq. 4)
SHETLAND (eq. 7)
(e)
HORDALAND (eq. 4)
CROMER KNOLL (eq. 6)
32/2-1

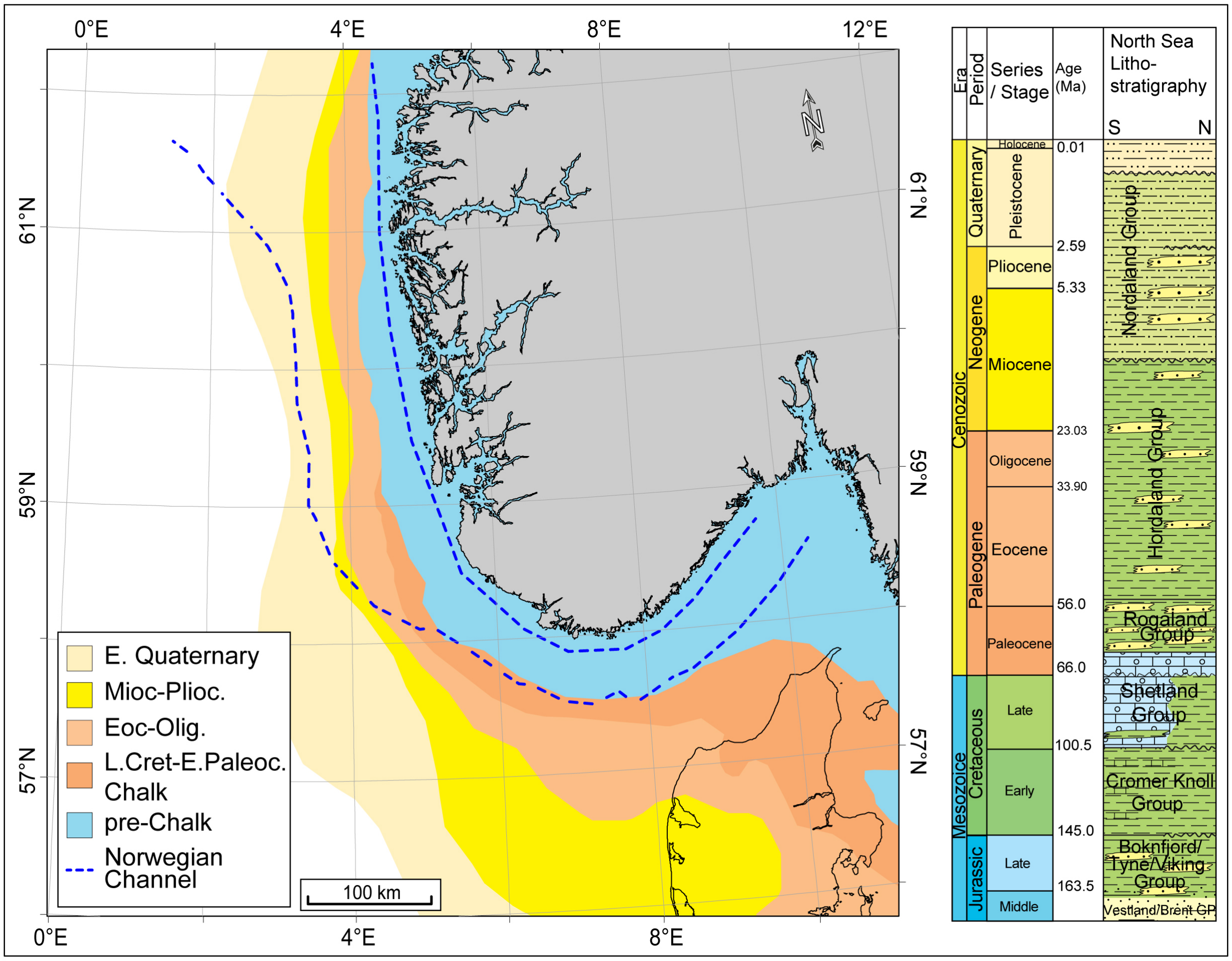

0°E
4°E
8°E
12°E
61°N
59°N
57°N
N
E. Quaternary
Mioc-Plioc.
Eoc-Olig.
L.Cret-E.Paleoc. Chalk
pre-Chalk
Norwegian Channel
100 km
Era
Period
Series / Stage
Age (Ma)
North Sea Litho-stratigraphy
S
N
Cenozoic
Quaternary
Holocene
Pleistocene
Neogene
Pliocene
Miocene
Paleogene
Oligocene
Eocene
Paleocene
Mesozoic
Cretaceous
Late
Early
Jurassic
Late
Middle
0.01
2.59
5.33
23.03
33.90
56.0
66.0
100.5
145.0
163.5
Nordaland Group
Hordaland Group
Rogaland Group
Shetland Group
Cromer Knoll Group
Boknfjord/ Tyne/Viking Group
Vestland/Brent GP

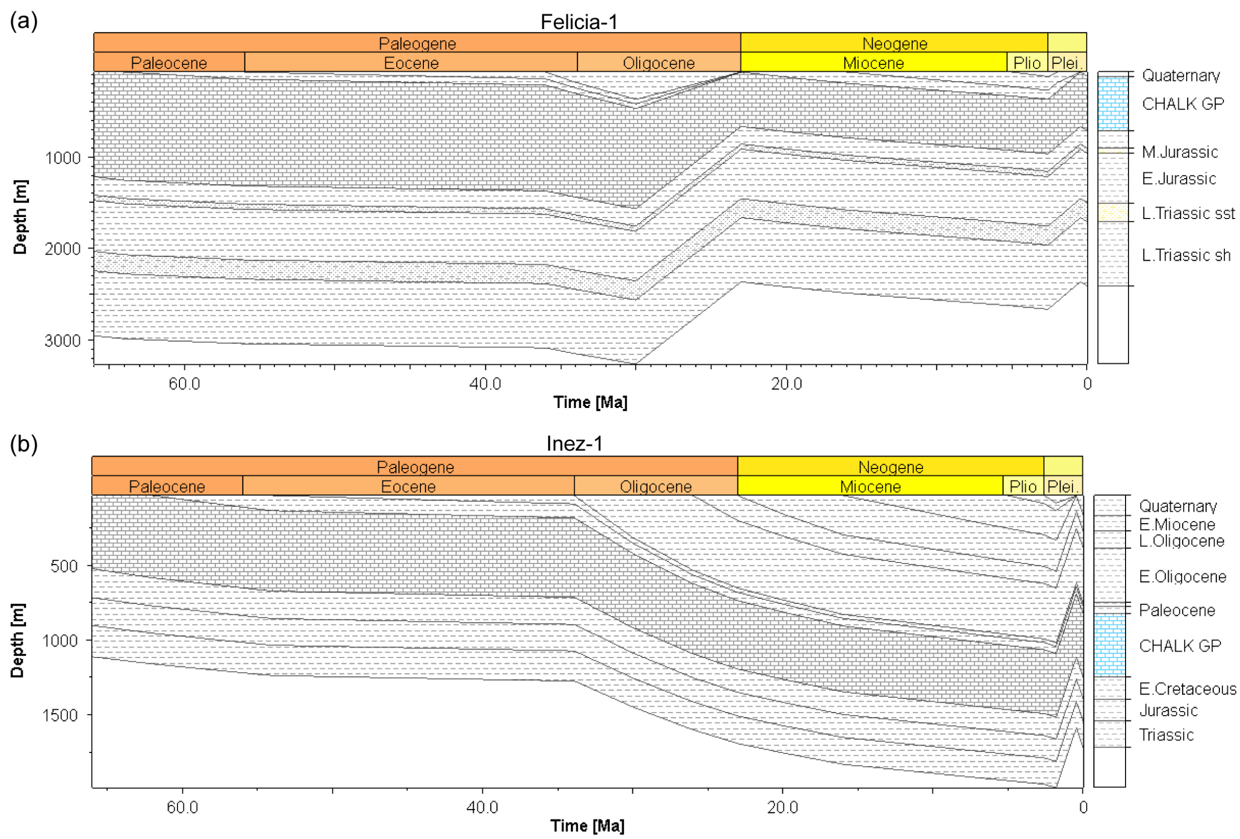
(a)
Felicia-1
Paleogene
Neogene
Paleocene
Eocene
Oligocene
Miocene
Plio
Plei.
Depth [m]
1000
2000
3000
60.0
40.0
20.0
0
Time [Ma]
Quaternary
CHALK GP
M.Jurassic
E.Jurassic
L.Triassic sst
L.Triassic sh
(b)
Inez-1
Paleogene
Neogene
Paleocene
Eocene
Oligocene
Miocene
Plio
Plei.
Depth [m]
500
1000
1500
60.0
40.0
20.0
0
Time [Ma]
Quaternary
E.Miocene
L.Oligocene
E.Oligocene
Paleocene
CHALK GP
E.Cretaceous
Jurassic
Triassic

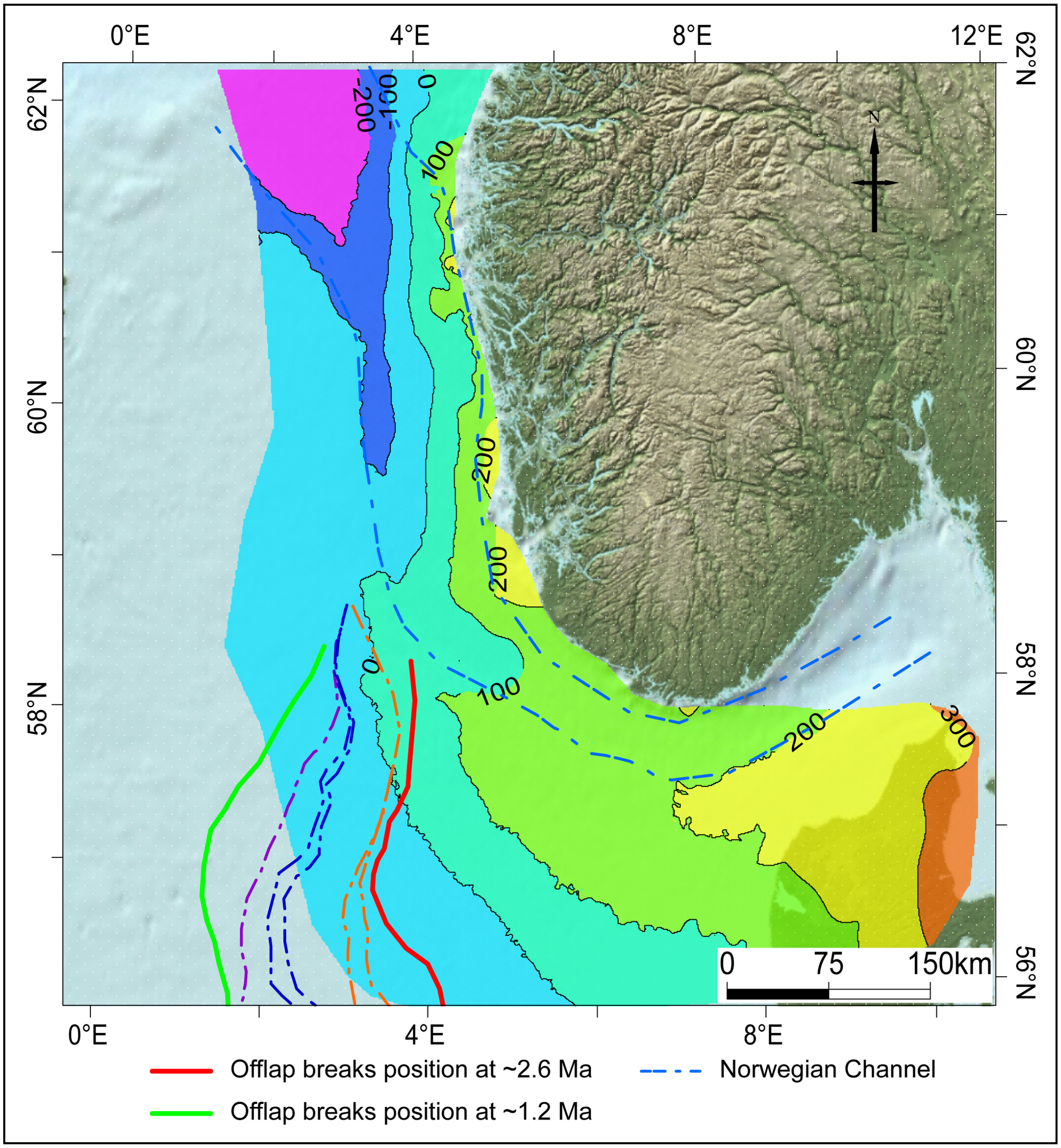

0°E
4°E
8°E
12°E
62°N
60°N
58°N
56°N
-200
-100
0
100
200
200
0
100
200
300
0
75
150km
Offlap breaks position at ~2.6 Ma
Offlap breaks position at ~1.2 Ma
Norwegian Channel

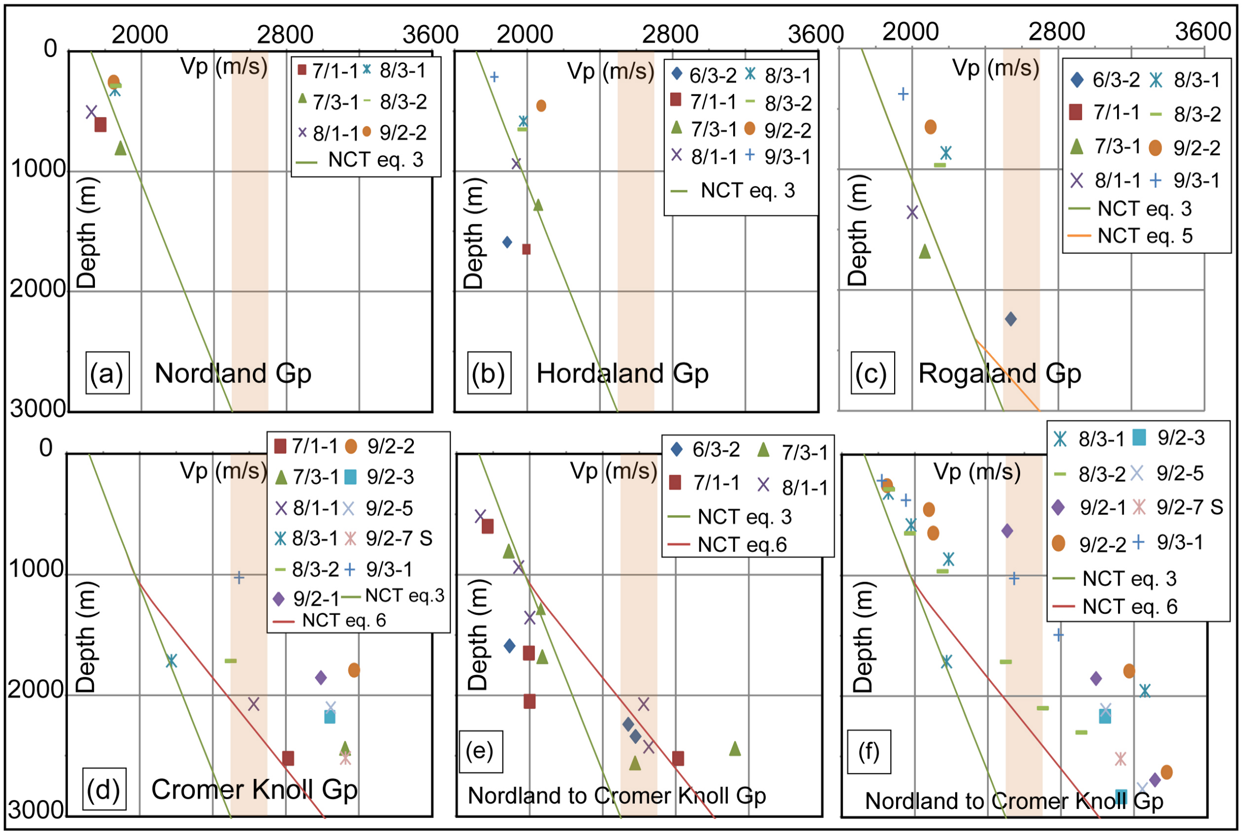

(a) Nordland Gp
(b) Hordaland Gp
(c) Rogaland Gp
(d) Cromer Knoll Gp
(e) Nordland to Cromer Knoll Gp
(f) Nordland to Cromer Knoll Gp
Vp (m/s)
Depth (m)
2000
2800
3600
0
1000
2000
3000
7/1-1
7/3-1
8/1-1
8/3-1
8/3-2
9/2-2
6/3-2
9/3-1
9/2-1
9/2-3
9/2-5
9/2-7 S
NCT eq. 3
NCT eq. 5
NCT eq. 6

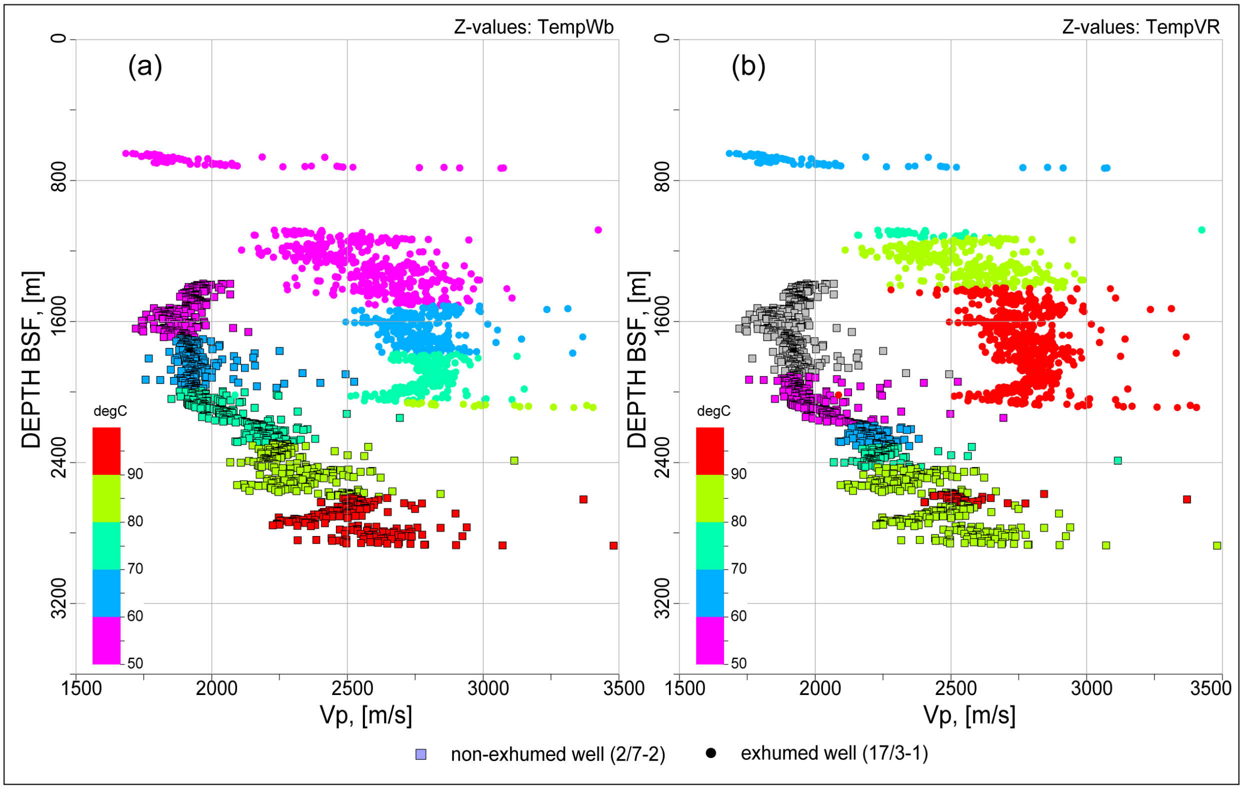

Z-values: TempWb
Z-values: TempVR
(a)
(b)
DEPTH BSF, [m]
0
800
1600
2400
3200
degC
90
80
70
60
50
1500
2000
2500
3000
3500
Vp, [m/s]
non-exhumed well (2/7-2)
exhumed well (17/3-1)

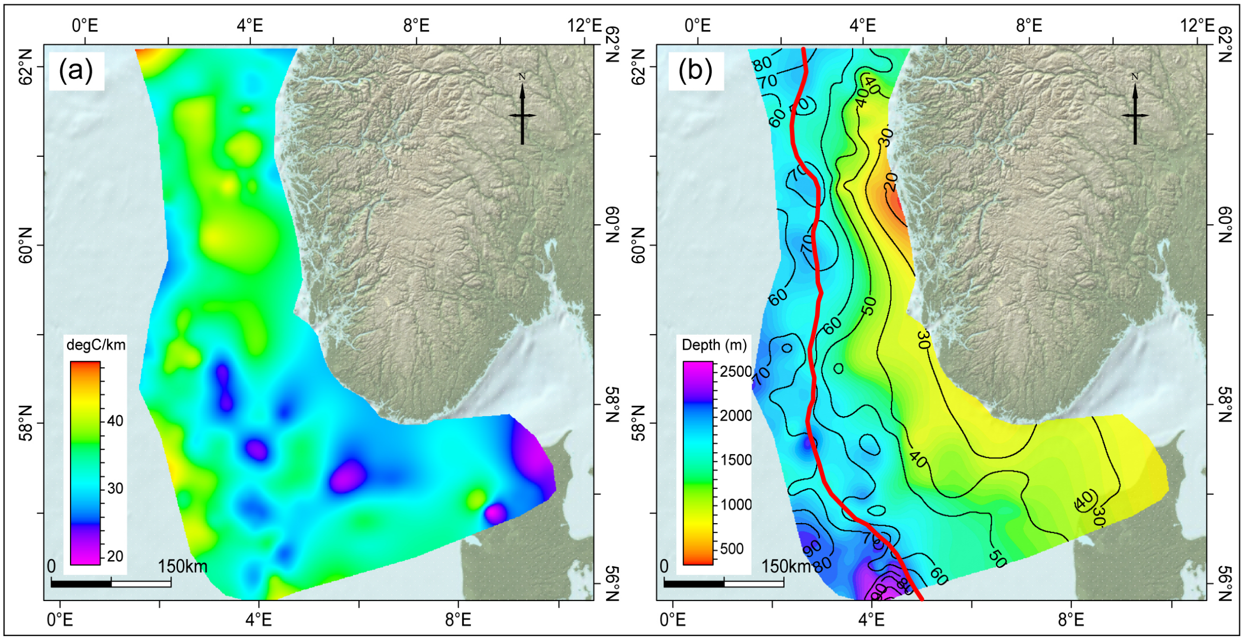

(a)
(b)
0°E
4°E
8°E
12°E
62°N
60°N
58°N
56°N
degC/km
40
30
20
Depth (m)
2500
2000
1500
1000
500
0
150km

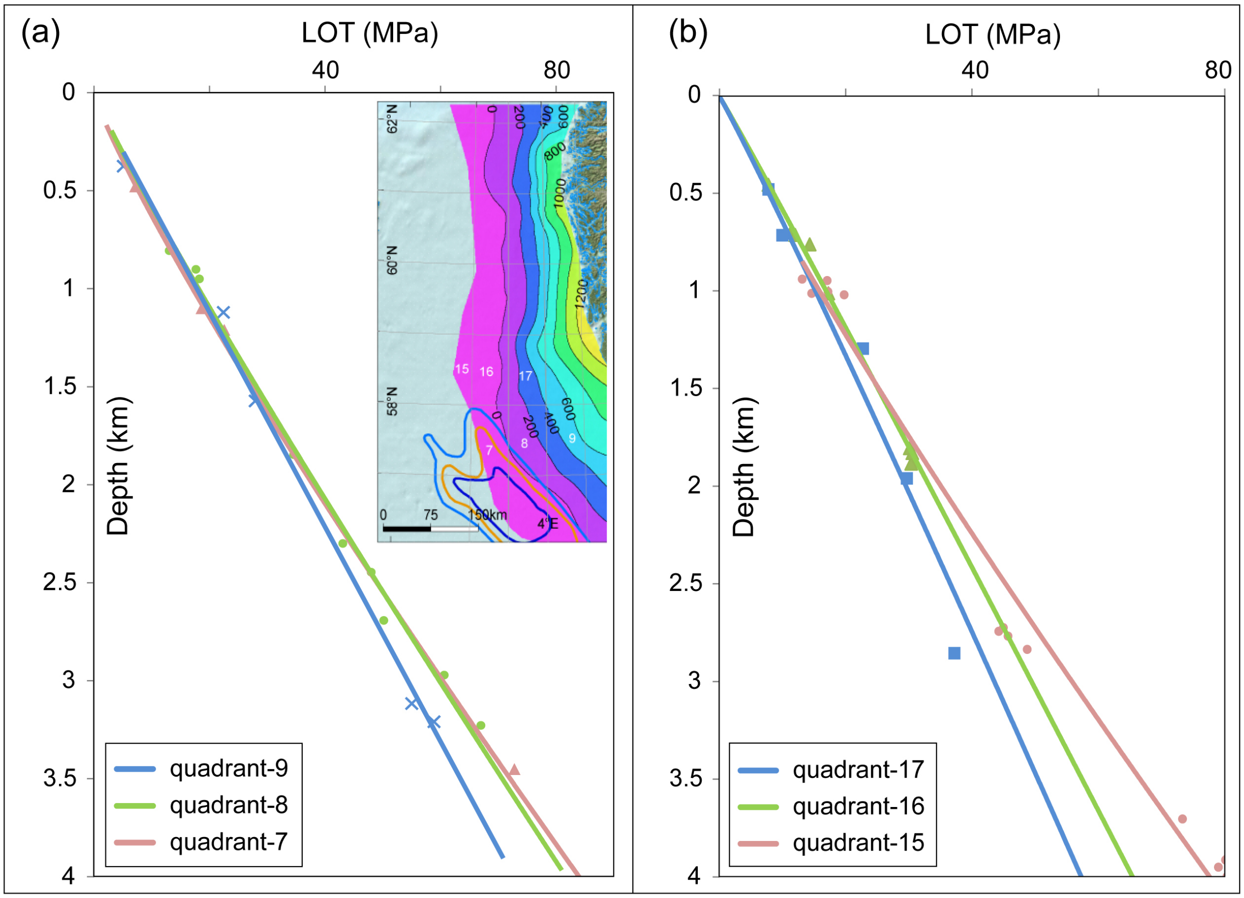
(a)
LOT (MPa)
40
80
0
0.5
1
1.5
2
2.5
3
3.5
4
Depth (km)
quadrant-9
quadrant-8
quadrant-7
62°N
60°N
58°N
0
200
400
600
800
1000
1200
15
16
17
7
8
9
0
75
150km
4°E
(b)
LOT (MPa)
40
80
Depth (km)
quadrant-17
quadrant-16
quadrant-15

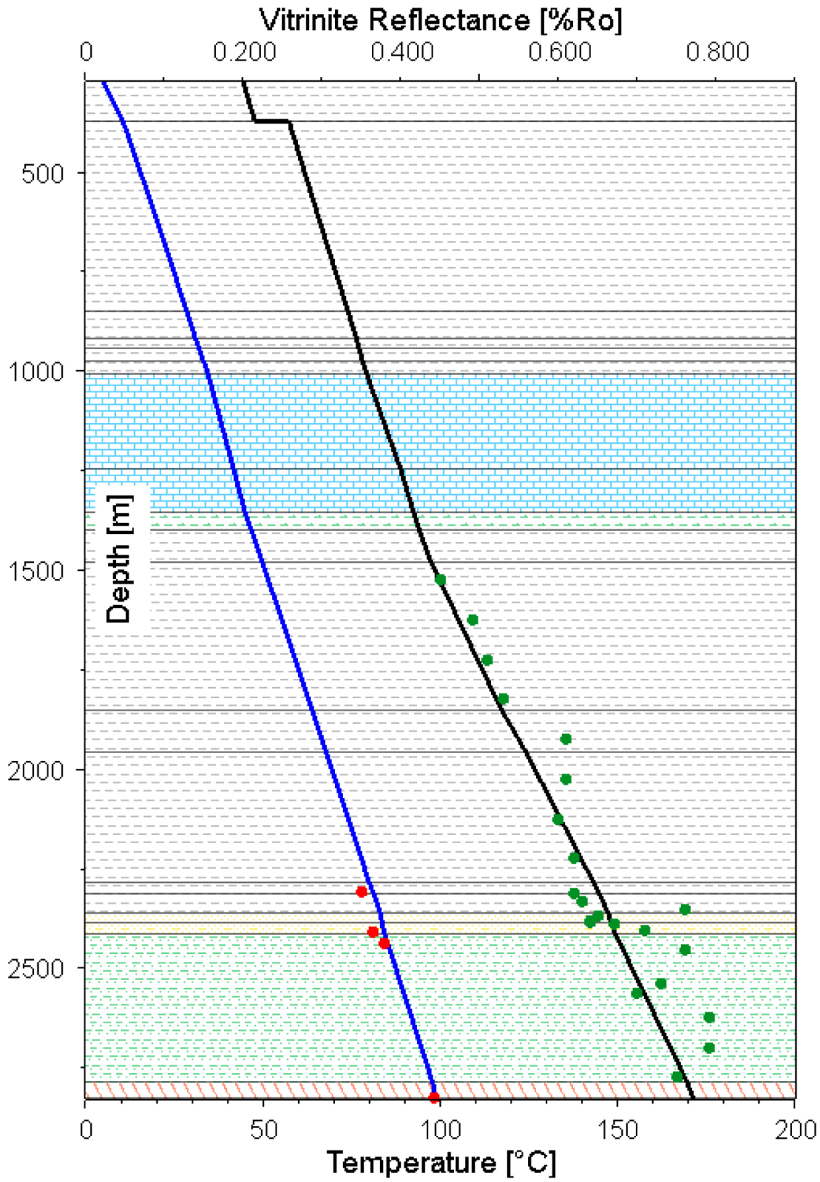
Vitrinite Reflectance [%Ro]
0
0.200
0.400
0.600
0.800
500
1000
1500
2000
2500
Depth [m]
0
50
100
150
200
Temperature [°C]

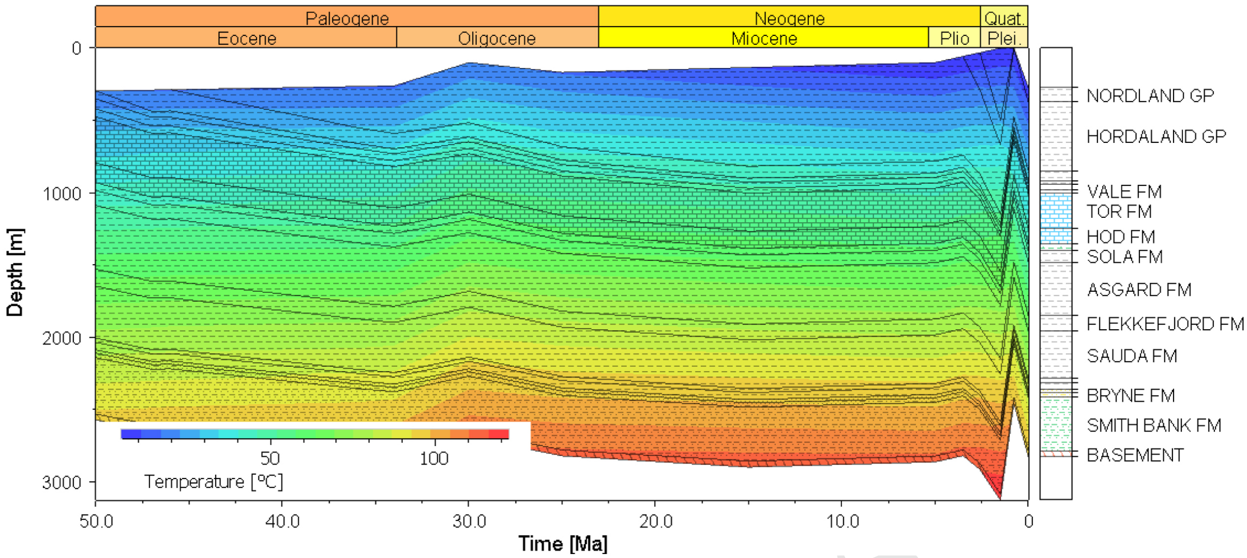
Paleogene
Neogene
Quat.
Eocene
Oligocene
Miocene
Plio
Plei.
Depth [m]
0
1000
2000
3000
Temperature [ºC]
50
100
Time [Ma]
50.0
40.0
30.0
20.0
10.0
0
NORDLAND GP
HORDALAND GP
VALE FM
TOR FM
HOD FM
SOLA FM
ASGARD FM
FLEKKEFJORD FM
SAUDA FM
BRYNE FM
SMITH BANK FM
BASEMENT

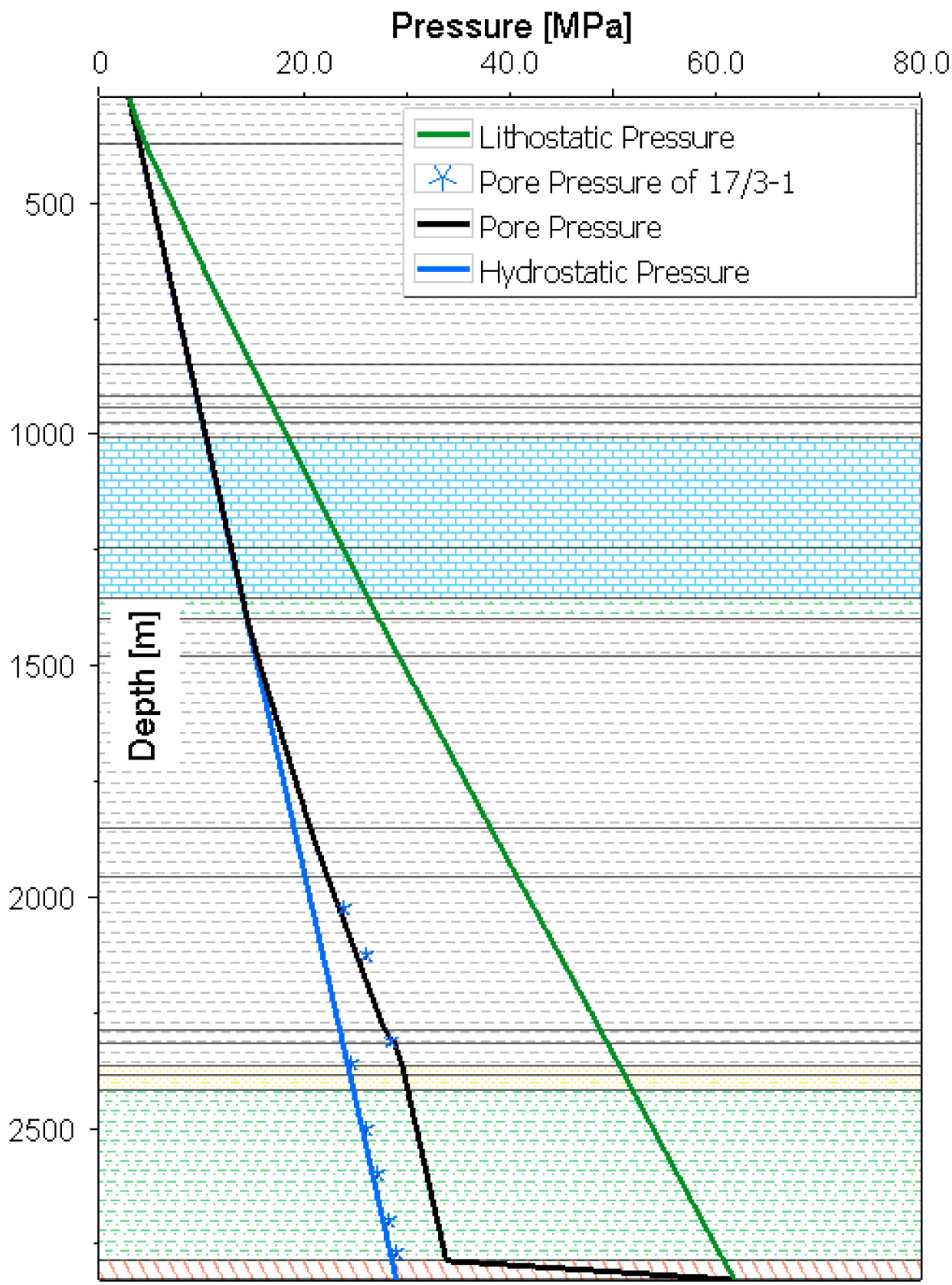
Pressure [MPa]
0
20.0
40.0
60.0
80.0
Depth [m]
500
1000
1500
2000
2500
Lithostatic Pressure
Pore Pressure of 17/3-1
Pore Pressure
Hydrostatic Pressure

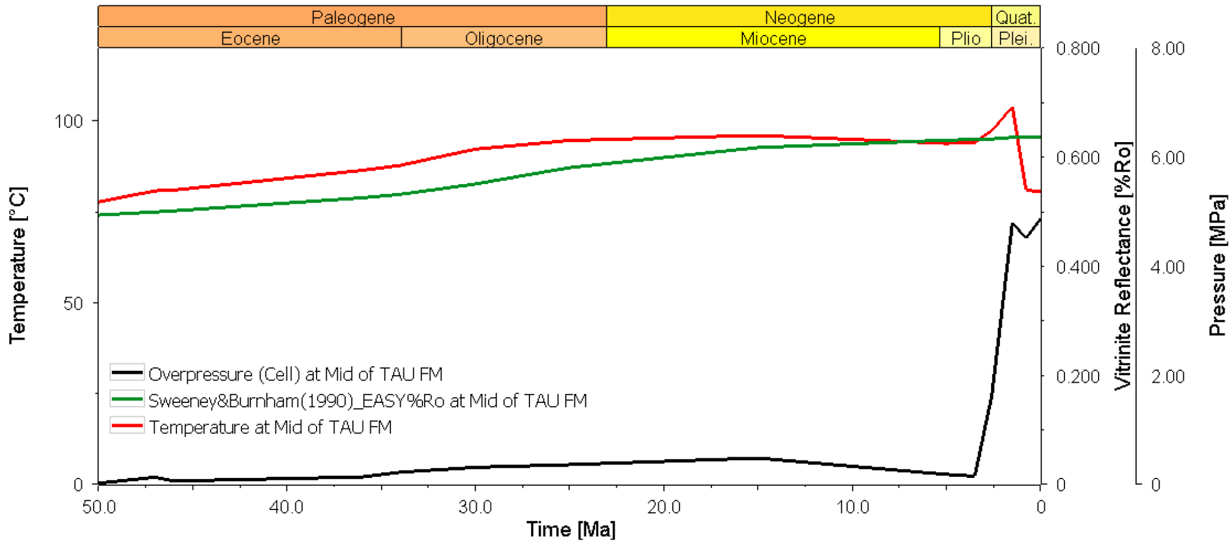

Paleogene
Neogene
Quat.
Eocene
Oligocene
Miocene
Plio
Plei.
Temperature [°C]
100
50
0
Vitrinite Reflectance [%Ro]
0.800
0.600
0.400
0.200
0
Pressure [MPa]
8.00
6.00
4.00
2.00
0
Overpressure (Cell) at Mid of TAU FM
Sweeney&Burnham(1990)_EASY%Ro at Mid of TAU FM
Temperature at Mid of TAU FM
50.0
40.0
30.0
20.0
10.0
0
Time [Ma]

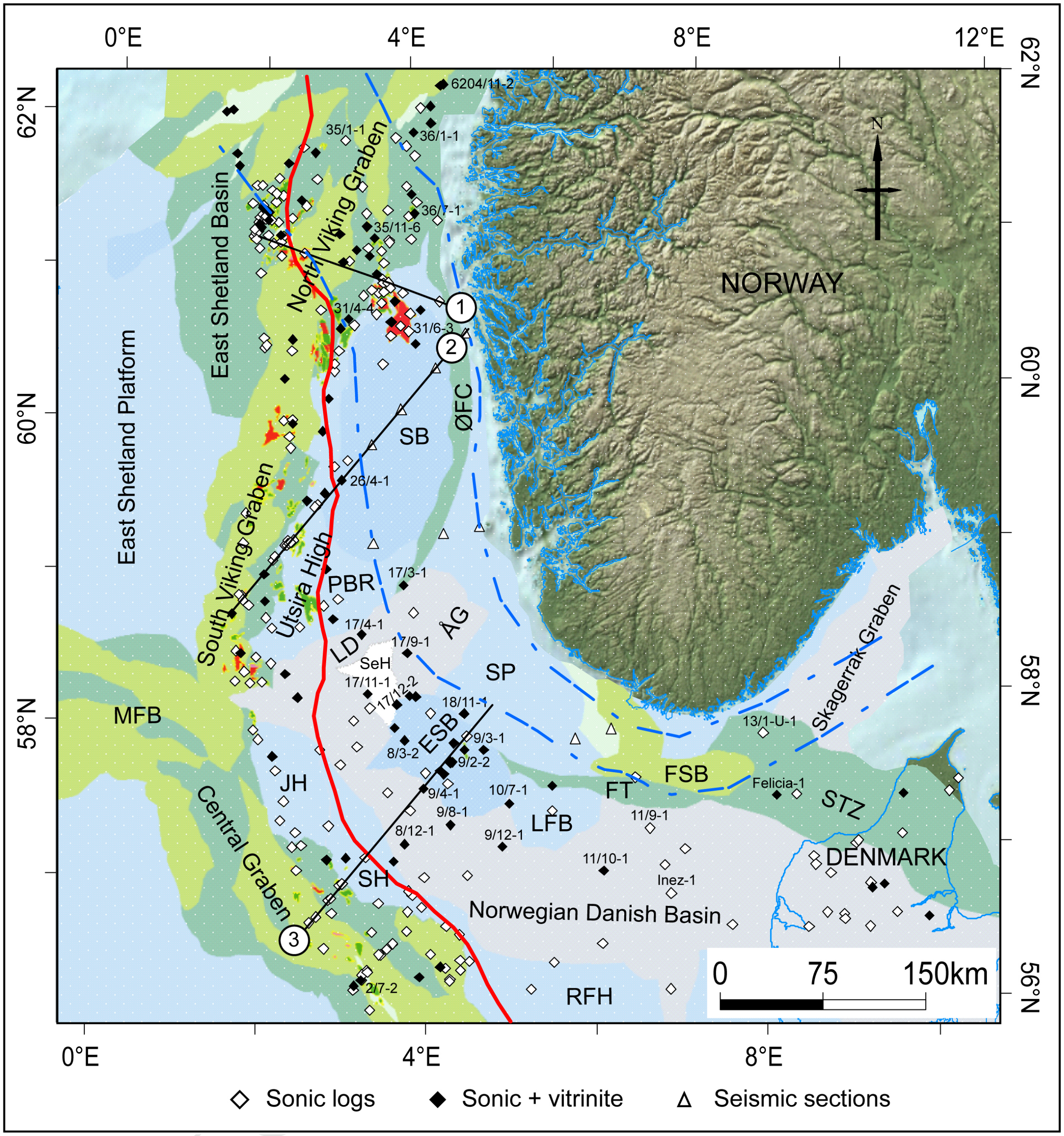

0°E
4°E
8°E
12°E
62°N
60°N
58°N
56°N
NORWAY
DENMARK
N
East Shetland Platform
East Shetland Basin
North Viking Graben
South Viking Graben
Utsira High
Central Graben
Skagerrak Graben
Norwegian Danish Basin
SB
ØFC
PBR
LD
SeH
AG
SP
ESB
JH
SH
MFB
FSB
FT
LFB
STZ
RFH
6204/11-2
35/1-1
36/1-1
36/7-1
35/11-6
31/4-4
31/6-3
26/4-1
17/3-1
17/4-1
17/9-1
17/11-1
17/12-2
18/11-1
9/3-1
9/2-2
8/3-2
9/4-1
10/7-1
9/8-1
8/12-1
9/12-1
11/9-1
11/10-1
Inez-1
13/1-U-1
Felicia-1
2/7-2
1
2
3
0
75
150km
Sonic logs
Sonic + vitrinite
Seismic sections

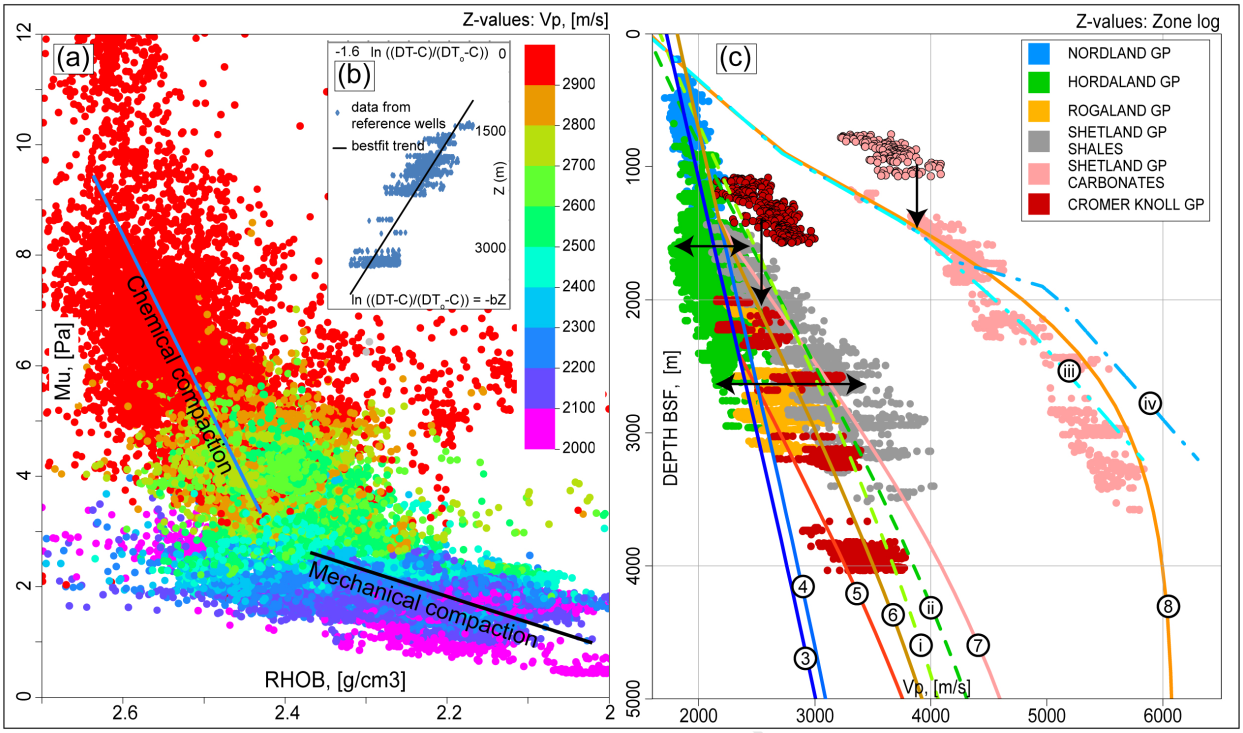

Z-values: Vp, [m/s]
(a)
(b)
-1.6 ln ((DT-C)/(DT$_o$-C)) 0
data from reference wells
bestfit trend
1500
3000
Z (m)
ln ((DT-C)/(DT$_o$-C)) = -bZ
2900
2800
2700
2600
2500
2400
2300
2200
2100
2000
Chemical compaction
Mechanical compaction
Mu, [Pa]
RHOB, [g/cm3]
Z-values: Zone log
(c)
NORDLAND GP
HORDALAND GP
ROGALAND GP
SHETLAND GP SHALES
SHETLAND GP CARBONATES
CROMER KNOLL GP
DEPTH BSF, [m]
Vp, [m/s]

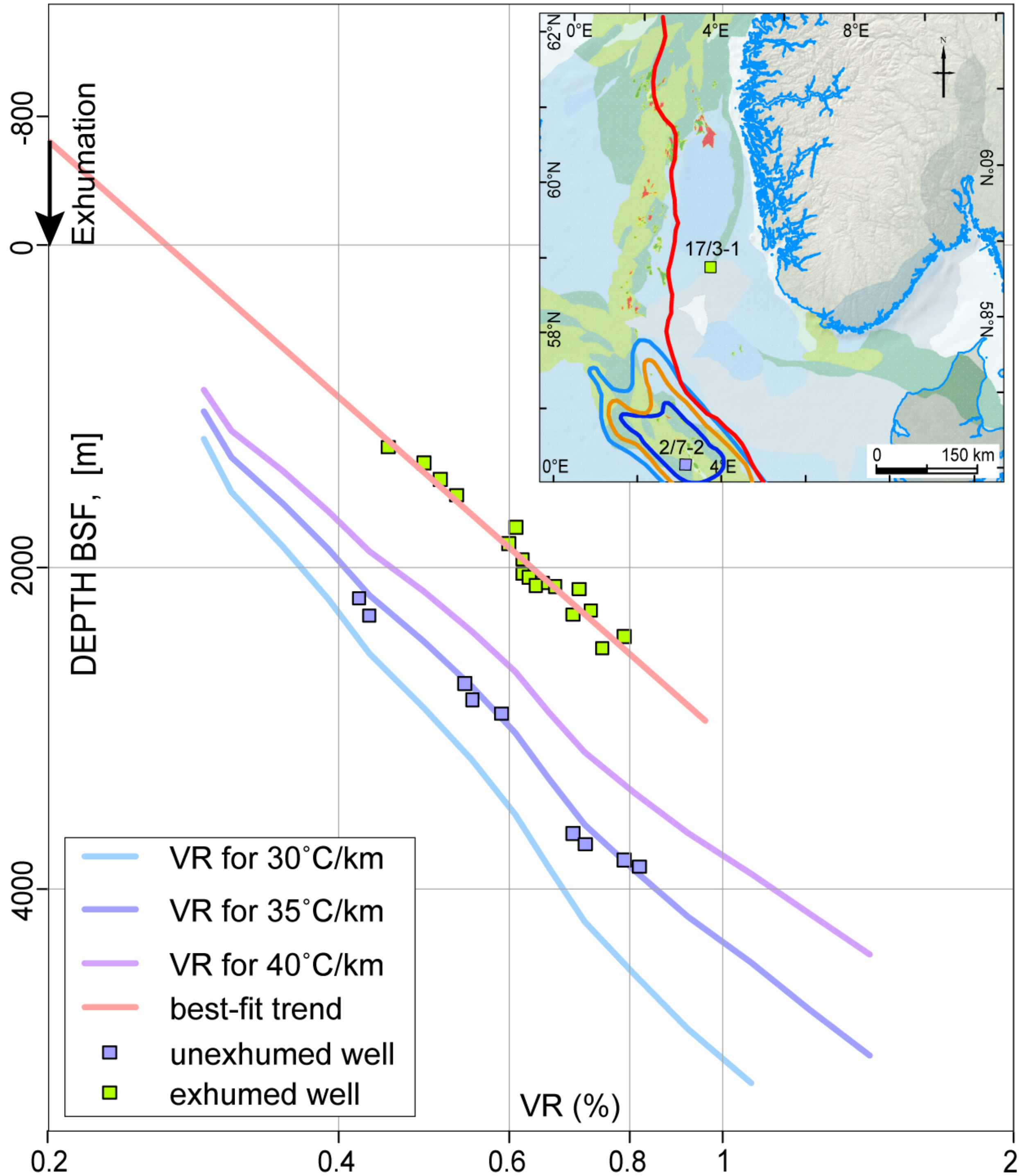

0°E
4°E
8°E
62°N
60°N
58°N
17/3-1
2/7-2
0
150 km
-800
0
2000
4000
Exhumation
DEPTH BSF, [m]
VR for 30˚C/km
VR for 35˚C/km
VR for 40˚C/km
best-fit trend
unexhumed well
exhumed well
VR (%)
0.2
0.4
0.6
0.8
1
2

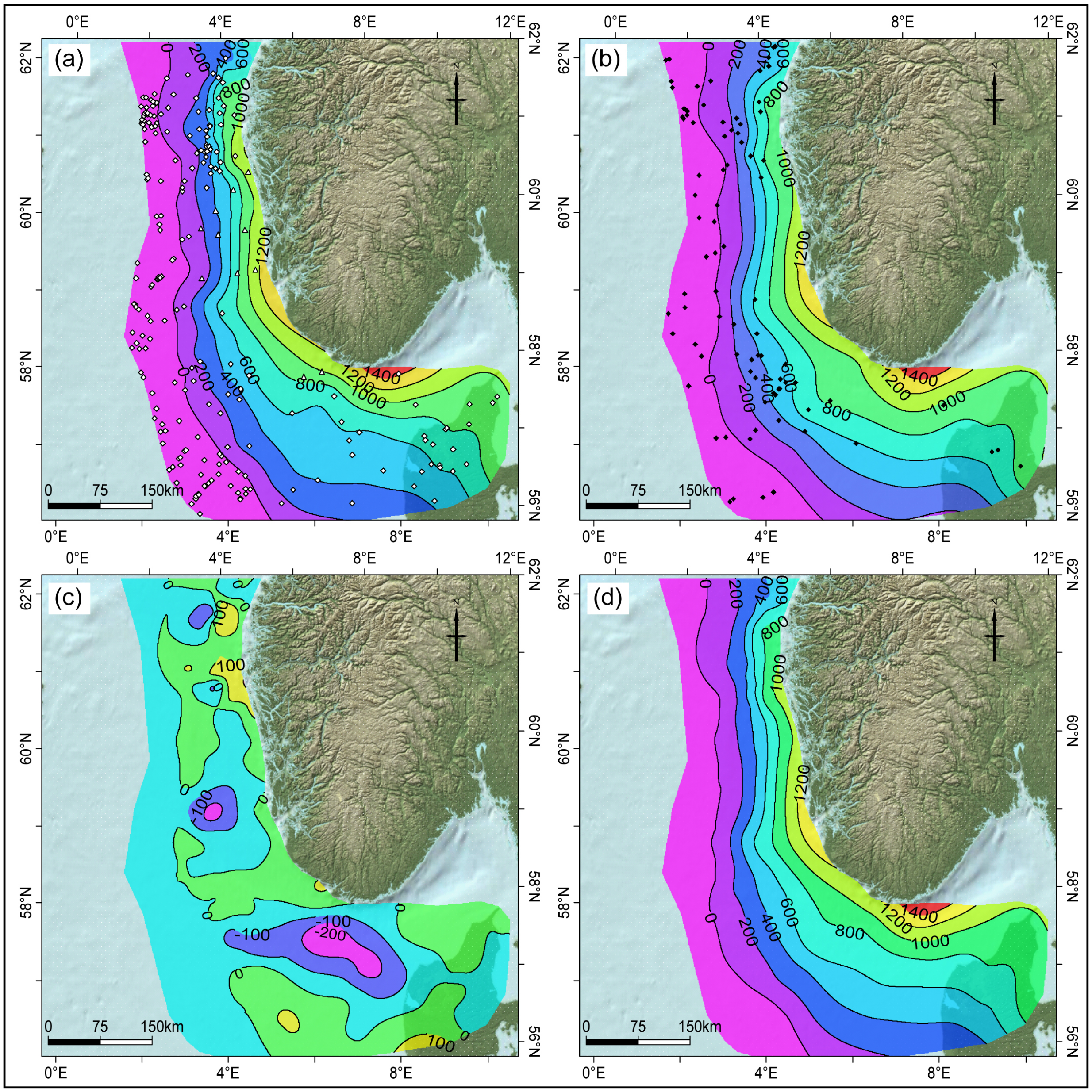
(a)
(b)
(c)
(d)
0°E
4°E
8°E
12°E
62°N
60°N
58°N
56°N
0
75
150km
0
200
400
600
800
1000
1200
1400
100
-100
-200

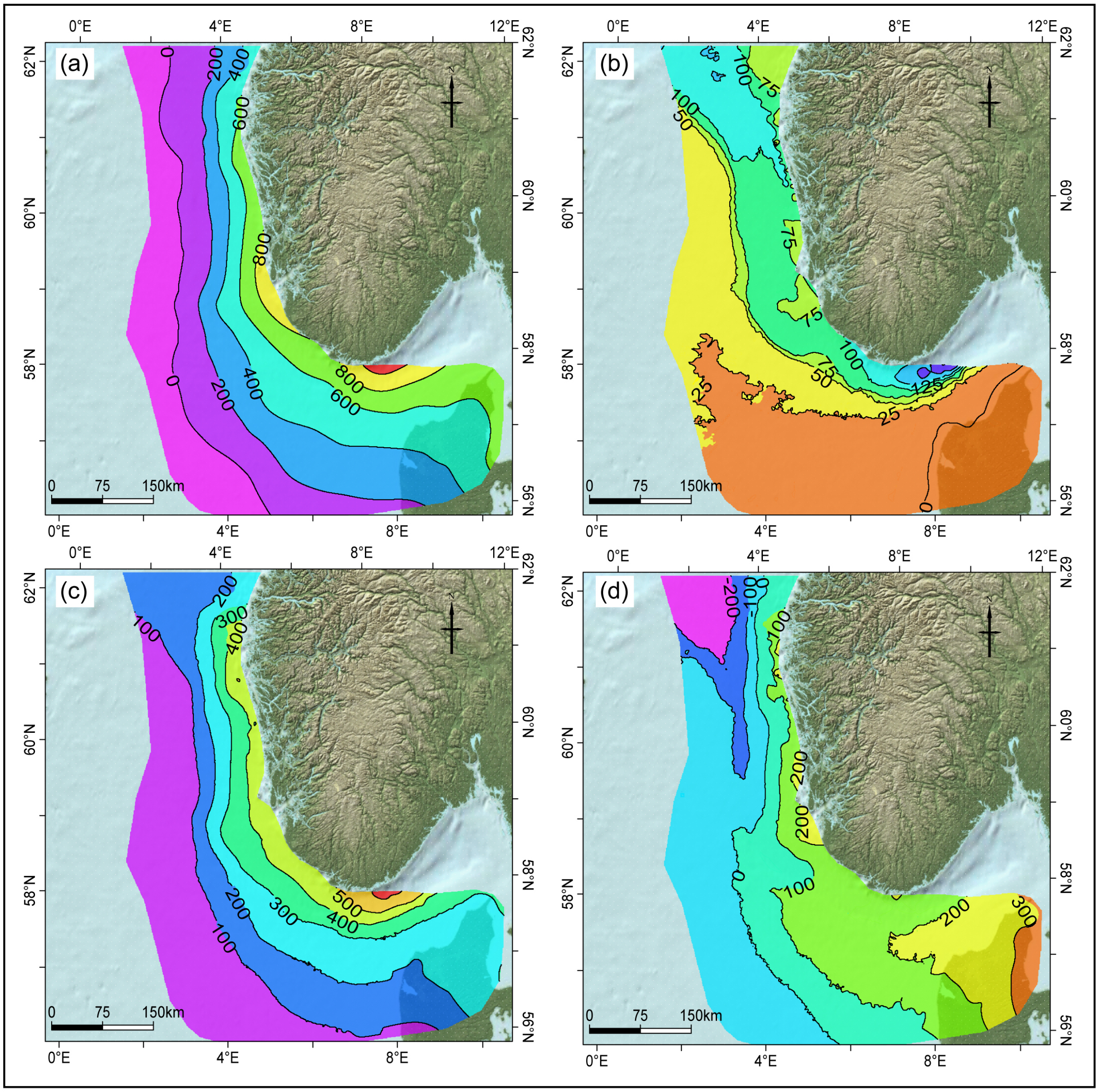
(a)
(b)
(c)
(d)
0°E
4°E
8°E
12°E
56°N
58°N
60°N
62°N
0
75
150km

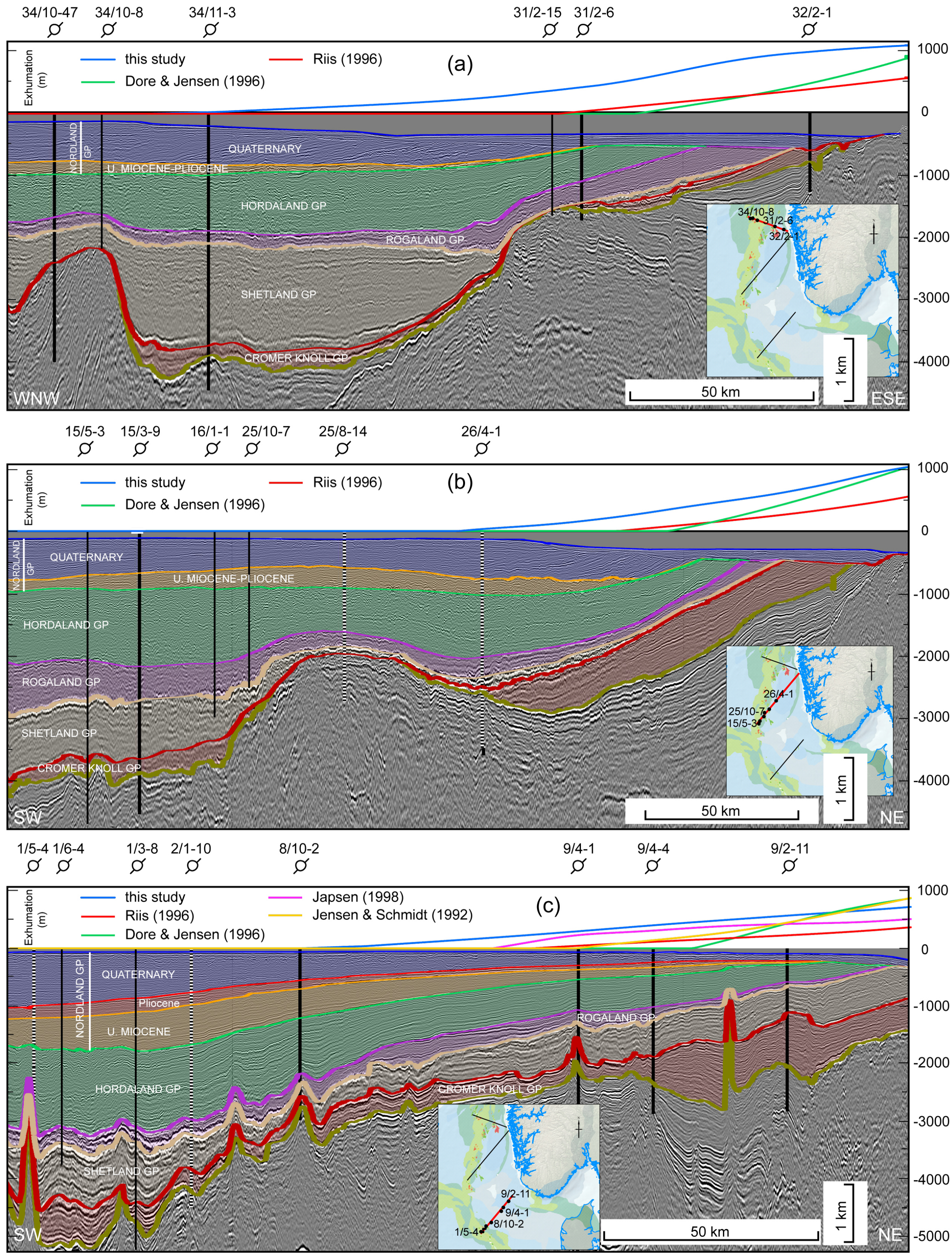
34/10-47
34/10-8
34/11-3
31/2-15
31/2-6
32/2-1
Exhumation (m)
this study
Riis (1996)
Dore & Jensen (1996)
(a)
1000
0
-1000
-2000
-3000
-4000
NORDLAND GP
QUATERNARY
U. MIOCENE-PLIOCENE
HORDALAND GP
ROGALAND GP
SHETLAND GP
CROMER KNOLL GP
WNW
ESE
50 km
1 km
15/5-3
15/3-9
16/1-1
25/10-7
25/8-14
26/4-1
(b)
SW
NE
1/5-4
1/6-4
1/3-8
2/1-10
8/10-2
9/4-1
9/4-4
9/2-11
Japsen (1998)
Jensen & Schmidt (1992)
(c)
Pliocene
U. MIOCENE
-5000

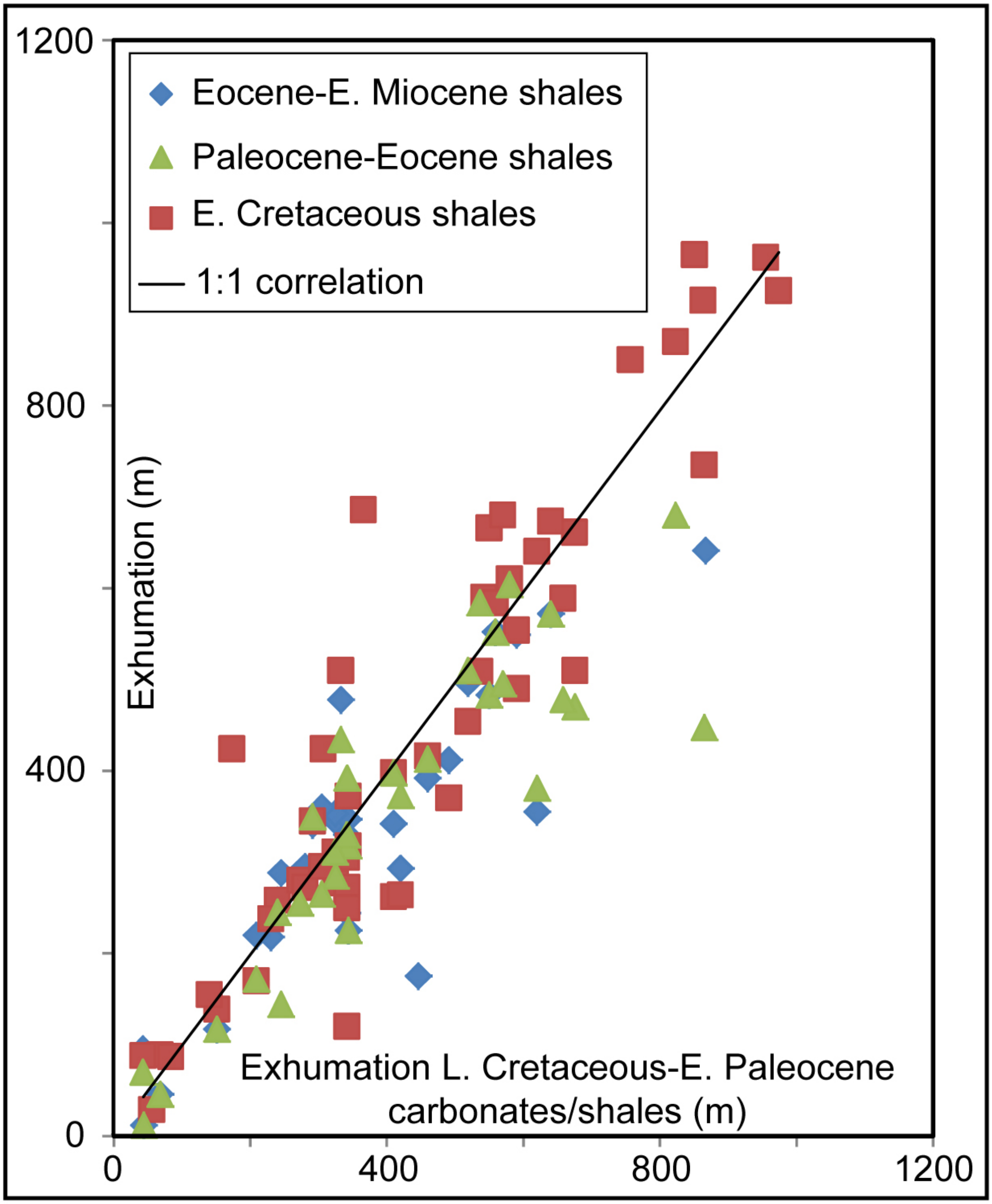

1200
800
400
0
0
400
800
1200
Eocene-E. Miocene shales
Paleocene-Eocene shales
E. Cretaceous shales
1:1 correlation
Exhumation (m)
Exhumation L. Cretaceous-E. Paleocene carbonates/shales (m)

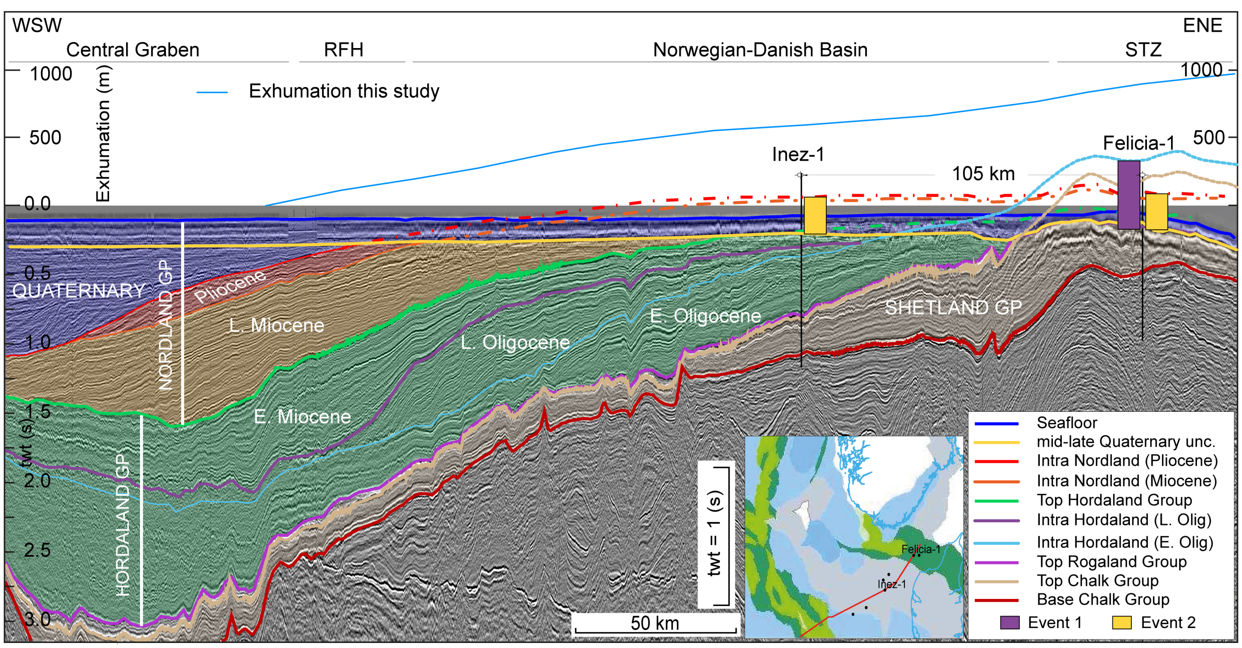
WSW
ENE
Central Graben
RFH
Norwegian-Danish Basin
STZ
Exhumation (m)
1000
500
0.0
Exhumation this study
Inez-1
105 km
Felicia-1
QUATERNARY
NORDLAND GP
Pliocene
L. Miocene
E. Miocene
L. Oligocene
E. Oligocene
SHETLAND GP
HORDALAND GP
twt (s)
0.5
1.0
1.5
2.0
2.5
3.0
twt = 1 (s)
50 km
Felicia-1
Inez-1
Seafloor
mid-late Quaternary unc.
Intra Nordland (Pliocene)
Intra Nordland (Miocene)
Top Hordaland Group
Intra Hordaland (L. Olig)
Intra Hordaland (E. Olig)
Top Rogaland Group
Top Chalk Group
Base Chalk Group
Event 1
Event 2

Highlights

- Exhumation estimated from compaction and thermal maturity based techniques
- Main tilting events during the Late Oligocene and late Plio-Pleistocene
- Rapid burial during the Quaternary may have contributed to high pore pressures in the Central and Viking Graben areas
- Reduced ratio of horizontal and vertical stresses on the basin margin areas
- Thermally immature source rocks on the basin margin areas